Alterations in microbial community composition with increasing fCO_2: a mesocosm study in the eastern Baltic Sea

Katharine J. Crawfurd[1], Santiago Alvarez-Fernandez[2], Kristina D. A. Mojica[3], Ulf Riebesell[4], Corina P. D. Brussaard[1,5]

[1]{NIOZ Royal Netherlands Institute for Sea Research, Department of Marine Microbiology and Biogeochemistry and Utrecht University, P.O. Box 59, 1790 AB Den Burg, Texel, The Netherlands}

[2]{Alfred-Wegener-Institut Helmholtz-Zentrum für Polar- und Meeresforschung, Biologische Anstalt Helgoland, 27498, Helgoland, Germany}

[3] {Department of Botany and Plant Pathology, Cordley Hall 2082, Oregon State University, Corvallis, Oregon 97331-29052, USA}

[4]{GEOMAR Helmholtz Centre for Ocean Research Kiel, Biological Oceanography, Düsternbrooker Weg 20, 24105, Kiel, Germany}

[5]{Aquatic Microbiology, Institute for Biodiversity and Ecosystem Dynamics, University of Amsterdam, P.O. Box 94248, 1090 GE Amsterdam, The Netherlands}

Correspondence to: K. Crawfurd (kate.crawfurd@gmail.com) and C. P. D. Brussaard (corina.brussaard@nioz.nl)

Abstract

Ocean acidification, resulting from the dissolution of anthropogenic carbon dioxide in the atmosphere, is considered a major threat to marine ecosystems. Here we examined effects of ocean acidification on microbial community dynamics in the eastern Baltic Sea, during the summer of 2012 when inorganic nitrogen and phosphorus were highly depleted. Large volume in situ mesocosms were employed to mimic present to future and far future CO_2 scenarios. All six groups of phytoplankton enumerated by flow cytometry (<20 µm cell diameter) showed distinct trends in net growth and abundance with CO_2 enrichment. The picoeukaryotic phytoplankton groups Pico-I and II displayed enhanced abundances, whilst Pico-III, *Synechococcus* and the nanoeukaryotic phytoplankton groups were negatively affected by elevated fCO_2. Specifically, the numerically dominant eukaryote, Pico-I, demonstrated increases in gross growth rate with increasing fCO_2 sufficient to double their abundances. Dynamics of the prokaryote community closely followed trends in total algal biomass despite differential effects of fCO_2 on algal groups. Similarly, viral abundances corresponded to prokaryotic host population dynamics. Viral lysis and grazing were both important in controlling microbial abundances. Overall our results point to a shift towards a more regenerative system with production dominated by small picoeukaryotic phytoplankton.

1 Introduction

Marine phytoplankton are responsible for approximately half of global primary production (Field et al., 1998), with shelf sea communities contributing an average 15-30 % (Kulinski and Pempkowiak, 2011). Since the industrial revolution atmospheric carbon dioxide (CO_2) concentrations have increased by nearly 40 % due to anthropogenic activities, primarily the burning of fossil fuels and deforestation (Doney et al., 2009). Atmospheric CO_2 dissolves in the oceans where it forms carbonic acid which reduces seawater pH, a process commonly termed, ocean acidification (OA). Currently,

along with warming sea surface temperatures and changing light and nutrient conditions, marine ecosystems face unprecedented decreases in ocean pH (Doney et al., 2009; Gruber, 2011). Ocean acidification is considered one of the greatest current threats to marine ecosystems (Turley and Boot, 2010) and has been shown to alter phytoplankton primary productivity with the direction and magnitude of the responses dependent on community composition (eg. Hein and Sand-Jensen, 1997; Tortell et al., 2002; Leonardos and Geider, 2005; Engel et al., 2007; Feng et al., 2009; Eberlein et al., 2017). Certain cyanobacteria, including diazotrophs, demonstrate stimulated growth under conditions of elevated CO_2 (Qiu and Gao, 2002; Barcelos e Ramos et al., 2007; Hutchins, 2007; Dutkiewicz et al., 2015). However, no consistent trends have been found for *Synechococcus* (Schulz et al., 2017 and references therein). The responses of diatoms and coccolithophores also appear more variable (Dutkiewicz et al., 2015 and references therein), although coccolithophore calcification seems generally negatively impacted (Meyer and Riebesell, 2015; Riebesell et al., 2017). OA has also been reported to increase the abundances of small-sized photoautotrophic eukaryotes in mesocosm experiments (Engel et al., 2007; Meakin and Wyman, 2011; Brussaard et al., 2013; Schulz et al., 2017).

Recently, data regarding the effects of OA on taxa-specific phytoplankton growth rates were incorporated into a global ecosystem model. The results emphasized that elevated CO_2 concentrations can cause changes in community structure by altering the competitive fitness, and thus competition between phytoplankton groups (Dutkiewicz et al., 2015). Moreover, OA was found to have a greater impact on phytoplankton community size structure, function and biomass than either warming or reduced nutrient supply (Dutkiewicz et al., 2015). Many OA studies have been conducted using single-species under controlled laboratory conditions and therefore cannot account for intrinsic community interactions that occur under natural conditions. Alternatively, larger-volume mesocosm experiments allow for OA manipulation of natural communities and as such, are more likely to capture and quantify the overall response of the natural ecosystems. To date, the majority of these experiments started under replete nutrient conditions or received nutrient additions (Paul et

al., 2015 and references therein). Thus, little data is available for oligotrophic conditions, which are present in ~75% of the world's oceans (Corno et al., 2007).

Whilst environmental factors such as temperature, light, nutrients and CO_2 concentration regulate gross primary production, loss factors determine the fate of this photosynthetically fixed carbon. Grazing, sinking and viral lysis affect the cycling of elements in different manners, i.e. transferred to higher trophic levels through grazing, carbon storage in sediments via sinking, and cellular content release by viral lysis (Wilhelm and Suttle, 1999; Brussaard et al., 2005). Released detrital and dissolved organic matter (DOM) is quickly utilized by heterotrophic bacteria, thereby stimulating activity within the microbial loop (Brussaard et al., 2008; Lønborg et al., 2013; Sheik et al., 2014; Middelboe and Lyck, 2002). Consequently, bacteria may be affected indirectly by OA through changes in the quality and/or quantity of DOM (Weinbauer et al., 2011). Viral lysis has been found to be as important as microzooplankton grazing to the mortality of natural bacterio- and phytoplankton (Weinbauer, 2004; Baudoux et al., 2006; Evans and Brussaard, 2012; Mojica et al., 2016). Thus far, most studies examining the effects of OA on microzooplankton abundance and/or grazing have found little or no direct effect (Suffrian et al., 2008; Rose et al., 2009; Aberle et al., 2013; Brussaard et al., 2013; Niehoff et al., 2013). To our knowledge, no viral lysis rates have been reported for natural phytoplankton communities under conditions of OA. A few studies have inferred rates based on changes in viral abundances under enhanced CO_2, but the results are inconsistent (Larsen et al., 2008; Brussaard et al., 2013). Therefore, the effect of OA on the relative share of these key loss processes is still understudied for most ecosystems.

Here we report on the temporal dynamics of microbes (phytoplankton, prokaryotes and viruses) under the influence of enhanced CO_2 concentrations in the low-salinity (around 5.7) Baltic Sea. Using large mesocosms under in situ light and temperature, the pelagic ecosystem was exposed to a range of increasing CO_2 concentrations from ambient to future and far future concentrations. The study was performed during the summer in the Baltic Sea near Tvärminne when conditions were oligotrophic. Our data show, that over the 43 day long experiment, enhanced CO_2 concentrations

105 elicited distinct shifts in the microbial community, most notably an increase in the net growth of
106 small picoeukaryotic phytoplankton.
107
108 **2 Materials and Methods**
109 **2.1 Study site and experimental set-up**
110 The present study was conducted in the Tvärminne Storfjärden (59° 51.5' N, 23° 15.5' E) between 14
111 June and 7 August, 2012. Nine mesocosms, each enclosing ~55 m^3 of water, were moored in a square
112 arrangement at a site with a water depth of approximately 30 m. The mesocosms consisted of open
113 ended polyurethane bags 2 m in diameter and 18.5 m in length mounted onto floating frames
114 covered at each end with a 3 mm mesh. Initially, the mesocosms were kept open for 5 days to allow
115 for rinsing and water exchange while excluding large organisms from entering with the 3 mm mesh.
116 During this time, the bags were positioned such that the tops were submerged 0.5 m below the
117 water surface and the bottoms hung down to 17 m depth in the water column. Photosynthetically
118 active radiation (PAR) transparent plastic hoods (open on the side) prevented rain and bird droppings
119 from entering the mesocosms, which would affect salinity and nutrients, respectively. Five days
120 before the CO_2 treatment was to begin, the water column of the mesocosms was isolated from the
121 influence of the surrounding water. To do so, the 3 mm mesh was removed and sediment traps (2 m
122 long) were attached to close off the bottom of the mesocosms. The top ends of the bags were raised
123 and secured to the frame 1.5 m above the water surface to prevent water entering via wave action.
124 The mesocosms were then bubbled with compressed air for 3.5 min, to remove salinity gradients and
125 ensure that the water body was fully homogeneous.
126 The present manuscript includes results from six of the original mesocosms, due to the unfortunate
127 loss of three mesocosms which were compromised by leakage. The mean fCO_2 during the
128 experiment, i.e. days 1-43, for the individual mesocosms were as follows: M1, 365 µatm; M3, 1007
129 µatm; M5, 368 µatm; M6, 821 µatm; M7, 497 µatm; M8, 1231 µatm (Table 1). The gradient of non-
130 replicated fCO_2 of the present study (as opposed to a smaller number of replicated treatment levels)

was selected as a balance between the necessary, but manageable, number of mesocosms and minimizing the impact of the high potential for loss of mesocosms to successfully address the underlying questions of the study (Schulz et al., 2013). Moreover, it maximizes the potential of identifying a threshold level concentration, if present (by allowing for a larger number of treatment levels). Carbon dioxide manipulation was carried out in four steps and took place between days 0 to 4 until the target fCO_2 was reached. Initial fugacity of CO_2 (fCO_2) was 240 µatm. For fCO_2 manipulations, 50 µm filtered natural seawater was saturated with CO_2 and then injected evenly throughout the depth of the mesocosms as described by Riebesell et al. (2013). Two mesocosms functioned as controls and were treated in a similar manner using only filtered seawater. On day 15, a supplementary fCO_2 addition was made to the top 7 m of mesocosms numbered 3, 6, and 8 to replace CO_2 lost due to outgassing (Paul et al., 2015; Spilling et al., 2016). Throughout this study we refer to fCO_2 which accounts for the non-ideal behavior of CO_2 gas and is considered the standard measurement required for gas exchange (Pfeil et al., 2012).

Initial nutrient concentrations were 0.05 µmol L^{-1}, 0.15 µmol L^{-1}, 6.2 µmol L^{-1} and 0.2 µmol L^{-1} for nitrate, phosphate, silicate and ammonium, respectively. Nutrient concentrations remained low for the duration of the experiment (Paul et al., 2015, this issue) and no nutrients were added. Salinity was relatively constant around 5.7. Temperature was more variable; on average temperature within the mesocosms (0-17 m) increased from ~8 °C to a maximum on day 15 of ~15 °C and then decreased again to ~8 °C by day 30. For further details of the experimental set-up, carbonate chemistry dynamics and nutrient concentrations throughout the experiment we refer to the general overview paper by Paul et al. (2015).

Collective sampling was performed every morning using depth integrated water samplers (IWS, HYDRO-BIOS, Kiel). These sampling devices were gently lowered through the water column collecting ~5 L of water gradually between 0-10 m (top) or 0-17 m (whole water column). Water was collected from all mesocosms and the surrounding water. Subsamples were obtained for enumeration of phytoplankton, prokaryotes and viruses. Samples for viral lysis and grazing experiments were taken

157 from 5 m depth using a gentle vacuum-driven pump system. Samples were protected against sunlight
158 and warming by thick black plastic bags containing wet ice. Samples were processed at in situ
159 temperature (representative of 5 m depth) under dim light and handled using nitrile gloves. As viral
160 lysis and grazing rates were determined from samples taken from 5 m depth, samples for microbial
161 abundances reported here were taken from the top 10 m integrated samples.
162 The experimental period has been divided into four phases based on major physical and biological
163 changes (Paul et al., 2015): Phase 0 before CO_2 addition (days -5 to 0), Phase I (days 1-16), Phase II
164 (days 17-30) and Phase III (days 31-43). Throughout this manuscript the data are presented using
165 three colors (blue, grey and red), representing low (mesocosms M1 and M5) intermediate (M6 and
166 M7) and high (M3 and M8) fCO_2 concentrations (Table 1).
167
168 **2.2 Microbial abundances**
169 Microbes were enumerated using a Becton Dickinson FACSCalibur flow cytometer (FCM) equipped
170 with a 488 nm argon laser. The samples were stored on wet ice and in the dark until counting. The
171 photoautotrophic cells (<20 µm) were counted directly using fresh seawater and were discriminated
172 by their autofluorescent pigments. Six phytoplankton clusters were differentiated based on the
173 bivariant plots of either chlorophyll (red autofluorescence) or phycoerythrin (orange
174 autofluorescence, for *Synechococcus* and Pico-III) against side scatter. The size of the different
175 phytoplankton clusters was determined by gentle filtration through 25 mm diameter polycarbonate
176 filters (Whatman) with a range of pore sizes (12, 10, 8, 5, 3, 2, 1, and 0.8 µm) according to Veldhuis
177 and Kraay (2004). Average cell sizes for the different phytoplankton groups were 1, 1, 3, 2.9, 5.2, and
178 8.8 µm diameter for the prokaryotic cyanobacteria *Synechococcus* spp. (SYN), picoeukaryotic
179 phytoplankton I, II and III (Pico-I-III), and nanoeukaryotic phytoplankton I, and II (Nano-I, II),
180 respectively. Pico-III was discriminated from Pico-II (comparable average cell size) by a higher orange
181 autofluorescence signature, potentially representing small-sized cryptophytes (Klaveness, 1989);
182 alternatively large single cells or microcolonies of *Synechococcus* (Haverkamp et al., 2009). The

cyanobacterial species *Prochlorococcus* spp. were not observed during this experiment. Counts were converted to cellular carbon by assuming a spherical shape equivalent to the average cell diameters determined from size fractionations and applying conversion factors of 237 fg C μm^{-3} (Worden et al., 2004) and 196.5 fg C μm^{-3} (Garrison et al., 2000) for pico- and nano-sized plankton, respectively. Microbial net growth and loss rates were derived from exponential regressions of changes in the cell abundances over time.

Abundances of prokaryotes and viruses were determined from 0.5 % glutaraldehyde fixed, flash frozen (-80 °C) samples according to Marie et al. (1999) and Brussaard (2004), respectively. The prokaryotes include heterotrophic bacteria, archaea and unicellular cyanobacteria, the latter accounting for maximal 10 % of the total abundance in our samples, as indicated by their autofluorescence. Briefly, thawed samples were diluted with sterile autoclaved Tris-EDTA buffer (10 mM Tris-HCl and 1 mM EDTA, pH 8.2; Mojica et al., 2014) and stained with the green fluorescent nucleic acid-specific dye SYBR-Green I (Invitrogen Inc.) to a final concentration of the commercial stock of 1.0×10^{-4} (for prokaryotes) or 0.5×10^{-4} (for viruses). Virus samples were stained at 80 °C for 10 min and then allowed to cool for 5 min at room temperature in the dark. Prokaryotes were stained for 15 min at room temperature in the dark (Brussaard, 2004). Prokaryotes and viruses were discriminated in bivariate scatter plots of green fluorescence versus side scatter. Final counts were corrected for blanks prepared and analyzed in a similar manner as the samples. Two groups of prokaryotes were identified by their stained nucleic acid fluorescence, referred here on as low (LNA) and high (HNA) fluorescence prokaryotes.

2.3 Viral lysis and grazing

Microzooplankton grazing and viral lysis of phytoplankton was determined using the modified dilution assay, based on reducing grazing and viral lysis mortality pressure in a serial manner allowing for increased phytoplankton growth (over the incubation period) with dilution (Mojica et al., 2016). Briefly, two dilution series were created in clear 1.2 L polycarbonate bottles by gently mixing 200 µm

sieved whole seawater with either 0.45 µm filtered seawater (i.e. microzooplankton grazers removed) or 30 KDa filtered seawater (i.e. grazers and viruses removed) to final dilutions of 20, 40, 70 and 100 %. The 0.45 µm filtrate was produced by gravity filtration of 200 µm mesh sieved seawater through a 0.45 µm Sartopore capsule filter. The 30 KDa ultrafiltrate was produced by tangential flow filtration of 200 µm pre-sieved seawater using a 30 kDa Vivaflow 200 PES membrane tangential flow cartridge (Vivascience). All treatments were performed in triplicate. Bottles were suspended next to the mesocosms in small cages at 5 m depth for 24 hours. Subsamples were taken at 0 and 24 h, and phytoplankton abundances of the grazing series (0.45 µm diluent) were enumerated by flow cytometry. Due to time constraint, the majority of the samples of the 30 kDa series were fixed with 1 % (final concentration) formaldehyde : hexamine solution (18 % v/v : 10 % w/v), for 30 min at 4 °C, flash frozen in liquid nitrogen and stored at –80 °C until flow cytometry analysis in the home laboratory. Fixation had no significant effect (student's t-tests, p-value >0.05) as tested periodically against fresh samples. The modified dilution assay was only run for Mesocosms 1 (low fCO_2) and 3 (high fCO_2) due to the logistics of handling times. Experiments were performed until day 31. Grazing rates and the combined rate of grazing and viral lysis were estimated from the slope of a regression of phytoplankton apparent growth versus dilution of the 0.45 µm and 30 kDa series, respectively. A significant difference between the two regression coefficients (as tested by analysis of covariance) indicated a significant viral lysis rate. Phytoplankton gross growth rate, in the absence of grazing and viral lysis, was derived from the y-intercept of the 30 kDa series regression. Similarly, significant differences between mesocosms M1 and M3 (low and high fCO_2) were determined through analysis of covariance of the dilution series for the two mesocosms. A significance threshold of 0.05 was used and significance is denoted throughout the manuscript by an asterisk (*). Occasionally, the regression of apparent growth rate versus fraction of natural water resulted in a positive slope (thus no reduction in mortality with dilution). In addition, very low phytoplankton abundances can also prohibit statistical significance of results. Under such conditions dilution

experiments were deemed unsuccessful (see for limitations of the modified dilution method, Baudoux et al., 2006; Kimmance and Brussaard, 2010; Stoecker et al., 2015).

Viral lysis of prokaryotes was determined according to the viral production assay (Wilhelm et al., 2002; Winget et al., 2005). After reduction of the natural virus concentration, new virus production by the natural bacterial community is sampled and tracked over time (24 h). Briefly, free viruses were reduced from a 300 ml sample of whole water by re-circulation over a 0.2 µm pore size polyether sulfone membrane (PES) tangential flow filter (Vivaflow 50, Vivascience) at a filtrate expulsion rate of 40 ml min^{-1}. The concentrated sample was then reconstituted to the original volume using virus-free seawater. This process was repeated a total of three times to gradually wash away viruses. After the final reconstitution, 50 ml aliquots were distributed into six polycarbonate tubes. Mitomycin C (Sigma-Aldrich) (final concentration, 1 µg ml^{-1}, maintained at 4 °C), which induces lysogenic bacteria (Weinbauer and Suttle, 1996) was added to a second series of triplicate samples for each mesocosm. A third series of incubations with 0.2 µm filtered samples was used as a control for viral loss (e.g. viruses adhering to the tube walls) and showed no significant loss of free viruses during the incubations. At the start of the experiment, 1 ml subsamples were immediately removed from each tube and fixed as previously described for viral and bacterial abundance. The samples were dark incubated at in situ temperature and 1 ml subsamples were taken at 3 h, 6 h, 9 h, 12 h and 24 h. Virus production was determined from linear regression of viral abundance over time. Viral production due to induction of lysogeny was calculated as the difference between production in the unamended samples and production of samples to which mitomycin C was added. Although mortality experiments were initially planned to be employed for mesocosms 1, 2, and 3 representing low, mid and high fCO_2 conditions, mesocosm 2 was compromised due to leakage. Additionally, due to logistical reasons assays were only performed until day 21.

To determine grazing rates on prokaryotes, fluorescently labeled bacteria (FLBs) were prepared from enriched natural bacterial assemblages (originating from the North Sea) labeled with 5-([4,6-Dichlorotriazin-2-yl]amino) fluorescein (DTAF, 36565 Sigma-Aldrich 40 µg ml^{-1}) according to Sherr et

al. (1993). Frozen ampoules of FLB (1-5 % of total bacterial abundance) were added to triplicate 1 L incubation bottles containing whole water gently passed through 200 µm mesh. Twenty ml samples were taken immediately after addition (0 h) and the headspace was removed by gently squeezing air from the bottle. The 1 L bottles were incubated on a slow turning wheel (1 rpm) at in situ light and temperature conditions (representative of 5 m depth) for 24 h. Sampling was repeated after 24 h. All samples were fixed to a 1 % final concentration of gluteraldehyde (0.2 µm filtered; 25 % EM-grade), stained (in the dark for 30 min at 4 °C) with 4',6-Diamidino-2-Phenylindole, Dihydrochloride (DAPI) solution (0.2 µm filtered; Acrodisc ®25 mm Syringe filters, PALL Life Sciences; 2 µg ml^{-1} final concentration; Sherr et al., 1993) and filtered onto 25 mm, 0.2 µm black polycarbonate filters (GE Healthcare life sciences). Filters were then mounted on microscopic slides and stored at -20 °C until analysis. FLBs present on a ~0.75 mm^2 area were counted using a Zeiss Axioplan 2 microscope. Grazing (µ d^{-1}) was measured according to $N_{T24} = N_{T0} * e^{-\mu t}$, where N_{T24} and N_{T0} are the number of FLBs present at 24 h and 0 h, respectively.

2.4 Statistics

Non-metric multidimensional scaling (NMDS) was used to follow microbial community development in each mesocosm over the experimental period. NMDS is an ordination technique which represents the dissimilarities obtained from an abundance data matrix in a *2*-dimensional space (Legendre and Legendre, 1998). In this case, the data matrix was comprised of abundance data for each phytoplankton group in each mesocosm for every day of sampling. The treatment effect was assessed by analysis of similarity (ANOSIM; Clarke, 1993) and inspection of the NMDS biplot. ANOSIM compares the mean of ranked dissimilarities of mesocosms between fCO_2 treatments (low: 1, 5, 7; high: 6, 3, 8) to the mean of ranked dissimilarities within treatments per phase. The NMDS plots allowed divergence periods in the development and community composition between treatments to be visually assessed (period 1 from day 3-13 and period 2 from days 16-24). Net growth rates of each of the different microbial groups were calculated for these identified divergence periods.

Relationships between net growth rates and peak cell abundances with fCO_2 were evaluated by linear regression against the average fCO_2 per mesocosm during each period or peak day. A generalized linear model was used to test the relationship between prokaryote abundance and carbon biomass with an ARMA correlation structure of order 3 to account for temporal autocorrelation. The model fulfilled all assumptions such as homoscedasticity and avoiding autocorrelation of the residuals (Zuur et al., 2007). A significance threshold of $p \leq 0.05$ was used and significance is denoted by an asterisk (*). All analyses were performed using the statistical software program R, using packages nlme (Pinheiro et al., 2017) and vegan (Oksanen et al., 2017) (R core Team, 2017). Where average of low and high mesocosm abundance data are reported, values represent the average of mesocosms 1, 5, 7 (mean fCO_2 365-497 µatm) and 6, 3, 8 (821-1231 µatm), respectively.

3 Results

3.1 Total phytoplankton dynamics in response to CO_2 enrichment

During Phase 0, low variability in phytoplankton abundances of the different mesocosms ($1.5 \pm 0.05 \times 10^5$ ml^{-1}) indicated good replicability of initial conditions prior to CO_2 manipulation (Fig. 1). This was further supported by the high similarity between microbial communities of the different mesocosms as indicated by the tight clustering of points in the NMDS plot during this period (Fig. 2). During Phase 0, the phytoplankton community (<20 µm) was dominated by pico-sized autotrophs, with the prokaryotic cyanobacteria *Synechococcus* (SYN) and Pico-I accounting for 69 % and 27 % of total abundance, respectively. After CO_2 addition, there were two primary peaks in phytoplankton, which occurred on day 4 in Phase I and day 24 in Phase II (Fig. 1a). The phytoplankton community became significantly different over time in the different treatments (ANOSIM, p=0.01, Fig. 2). Two periods were identified based on their divergence (Fig.2), the first (NMDS-based period 1) followed the initial peak in abundance (days 3-13) with highest abundances occurring in the elevated CO_2 mesocosms (Fig. 1a). During the second period (NMDS-based period 2, days 16-24), abundances were higher in

312 the low fCO_2 mesocosms (Fig. 1a). In general the NMDS plot shows that throughout the experiment,
313 mesocosm M1 followed the same basic trajectory as mesocosms M5 and M7, whilst mesocosm M3
314 followed M6 and M8 (Fig. 2). Thus, the two mesocosms (representing high and low fCO_2 treatments)
315 deviated from each other during Phase I and were clearly separated during Phases II and III (Fig. 2).
316 Phytoplankton abundances in the surrounding water started to differ from the mesocosms during
317 Phase 0 (on average 44 % lower) which was primarily due to lower abundances of SYN. This effect
318 was seen from day -1, prior to CO_2 addition but following bubbling with compressed air (day -5). On
319 day 15, a deep mixing event occurred as a result of storm conditions (with consequent alterations in
320 temperature and salinity) and as a result phytoplankton abundances in the surrounding open water
321 diverged more strongly from the mesocosms but remained similar in their dynamics (Fig. 3).
322 Microbial abundances in the 0-17 m samples were slightly lower but showed very similar dynamics to
323 those in the 0-10 m samples (Fig. S1).
324
325 **3.1.1 *Synechococcus***
326 The prokaryotic cyanobacteria *Synechococcus* (SYN) accounted for the majority of total abundance,
327 i.e. 74 % averaged across all mesocosms over the experimental period. Abundances of SYN showed
328 distinct variability between the different CO_2 treatments, starting on day 7, with the low CO_2
329 mesocosms exhibiting nearly 20 % lower abundances between days 11-15 as compared to high fCO_2
330 mesocosms (Fig. 3a). SYN net growth rates during days 3-13 (NMDS-based period 1) were positively
331 correlated with CO_2 ($p=0.10$, $R^2=0.53$; Table 2, Fig. S2a). One explanation for higher net growth rates
332 at elevated CO_2 could be the significantly ($p<0.05$) higher grazing rate in the low fCO_2 mesocosm M1
333 (0.56 d^{-1}) compared to the high fCO_2 M3 (0.27 d^{-1}) as measured on day 10 (Fig. 4a). After day 16, SYN
334 abundances increased in all mesocosms and during this period (days 16-24) net growth rates had a
335 significant negative correlation to fCO_2 ($p=0.05$, $R^2= 0.63$; Figs. 3a, Table 2 and Fig. S3a).
336 Consequently, the net increase in SYN abundances during this period was on average 20 % higher at
337 low compared to high fCO_2. This corresponded to higher total loss rates in high fCO_2 treatments

measured on day 17 (0.33 vs 0.17 d^{-1} for M3 and M1, respectively; Fig. 4a). The higher net growth most likely led to the peak in SYN abundance observed on day 24 (max. 4.7 x 10^5 ml^{-1}), which was negatively correlated with fCO_2 (p=0.01, R^2=0.80; Table 3, Fig. S4a). After this period (days 24-28), SYN abundances declined at comparable rates in the different mesocosms, irrespective of fCO_2 (Fig. 3a). Abundances in the low fCO_2 mesocosms remained higher into Phase III (Fig. 3a). SYN abundances in the surrounding water were generally lower than in the mesocosms, with the exception of days 17-21.

3.1.2 Picoeukaryotes

In contrast to the prokaryotic photoautotrophs, the eukaryotic phytoplankton community showed a strong positive response to elevated fCO_2 (Fig. 1b). Pico-I was the numerically dominant group of eukaryotic phytoplankton, accounting for an average 21-26 % of total phytoplankton abundances. Net growth rates leading up to the first peak in abundance (from day 1 to 5) had a strong positive correlation with fCO_2 (p<0.01, R^2=0.90; Fig. 3b, Table 3, Fig. S5a). Accordingly, the peak on day 5 (max. 1.1 x 10^5 ml^{-1}; Fig. 3b) was also correlated positively with fCO_2 (p=0.01, R^2=0.81; Table 3, Fig. S4b). During Phase I, from days 3-13 (i.e. NMDS-based period 1), net growth rates of Pico-I remained positively correlated to CO_2 concentration (p=0.01, R^2=0.80; Table 2, Fig. S2b). However, during this period there was also a decline in abundance (days 5-9; p<0.01, R^2=0.89; Table 3, Fig. S5b) with 23 % more cells lost in the low fCO_2 mesocosms. Accordingly, following this period, gross growth rate was significantly higher in the high fCO_2 mesocosm M3 as compared to the low fCO_2 mesocosm M1 (day 10, p<0.05; Fig. 4b). Pico-I abundances in the surrounding open water started to deviate from the mesocosms after day 10, and were on average around half that of the low fCO_2 mesocosms (Fig. 3b). Following a brief increase (occurring between days 11-13) correlated to fCO_2 (p<0.01, R^2=0.94; Table 3, Fig. S4c), abundances declined sharply between days 13-16 (Fig. 3b), coinciding with a significantly higher total mortality rate in the high fCO_2 mesocosm M3 (day 13; Fig. 4b). Viral lysis was a substantial loss factor relative to grazing, for this group, comprising an average 45 % and 70 % of

364 total losses in M1 and M3, respectively (Table S1). During NMDS-based period 2, net growth rates of
365 Pico-I were significantly higher at high fCO_2 (p=0.05, R^2=0.64; Table 2, Fig S3b). By day 21,
366 abundances in the high fCO_2 mesocosms were (on average) ~2-fold higher than at low fCO_2
367 (maximum abundances 8.7 x 10^4 ml^{-1} and 5.9 x 10^4 ml^{-1} for high and low fCO_2 mesocosms; p=0.01,
368 R^2=0.84; Table 3, Fig. S4d). Standing stock of Pico-I remained high in the elevated fCO_2 mesocosms
369 for the remainder of the experiment (7.9 x 10^4 vs 4.3 x 10^4 ml^{-1} on average for high and low fCO_2
370 mesocosms, respectively; Fig. 3b). Additionally, gross growth rates during this final period were
371 relatively low (0.14 and 0.16 d^{-1} in M1 and M3, respectively) and comparable to total loss rates
372 (averaging 0.13 and 0.10 d^{-1} over days 25-31, for M1 and M3, respectively; Fig. 4b).
373 Another pico-eukaryote group, Pico-II, slowly increased in abundance until day 13, when it increased
374 more rapidly (Fig. 3c). Gross growth rates measured during Phase I were high (0.69 and 0.72 d^{-1} on
375 average in the low and high fCO_2 mesocosms M1 and M3, respectively; Fig. 4c), and comparable to
376 loss processes (0.46 and 0.58 d^{-1}), indicative of a relatively high turnover rate of production. Overall
377 net growth rates during days 3-13 (NMDS-based period 1) did not correlate to CO_2 (p=0.52, R^2=0.11;
378 Table 2, Fig. S2c). However, during periods of rapid increases in net growth, abundances were
379 positively correlated to CO_2 concentration (days 12-17; p=0.01, R^2=0.82; Table 3, Fig. S5c).
380 Accordingly, the peak in abundances of Pico-II on day 17 displayed a distinct positive correlation with
381 fCO_2 (p<0.01, R^2=0.93; Table 3, Fig. S4e), with maximum abundances of 4.6 x 10^3 ml^{-1} and 3.4 x 10^3
382 ml^{-1} for the high and low fCO_2 mecososms, respectively (Fig. 3c). In M8 (the highest fCO_2 mesocosm),
383 abundances increased for an extra day with the peak occurring on day 18, resulting in an average 23
384 % higher abundances. During the decline of the Pico-II peak (days 16-24), net growth rates were
385 negatively correlated with fCO_2 (p=0.10, R^2=0.52; Table 2, Fig S3c). Moreover, the rate of decline was
386 faster for the high fCO_2 mesocosms during days 18-21 (p<0.01, R^2=0.85). The Pico-II abundances in
387 the surrounding water were comparable to the mesocosms during Phases 0 and I, lower during
388 Phase II and higher during Phase III (Fig. 3c).

389 Pico-III exhibited a short initial increase in abundances in the low fCO_2 treatments, resulting in nearly
390 2-fold higher abundances at low fCO_2 by day 3 compared to the high fCO_2 treatment (Fig. 3d). After
391 this initial period, net growth rates of this group had a significant positive correlation with fCO_2 (days
392 3-13; p=0.04, R^2=0.67; Table 2, Fig. S2d). In general, during Phase I gross growth (p<0.01, days 1, 3,
393 10; Fig. 4d) and total mortality (p<0.05, days 1, 6, 10; Fig. 4d) were significantly higher in the low fCO_2
394 mesocosm M1, as compared to the high fCO_2 mesocosm M3 resulting in low net growth rates. During
395 Phase II (days 16-24, NMDS-based period 2) the opposite occurred; i.e. net growth rates were
396 negatively correlated with fCO_2 (p<0.01, R^2=0.86; Table 2, Fig S.3d). Maximum Pico-III abundances
397 (day 24: 4.2 x 10^3 and 8.3 x 10^3 ml^{-1} for high and low fCO_2) had a strong negative correlation with fCO_2
398 (p<0.01, R^2=0.91; Table 3, Fig. S4f). Pico-III abundances remained noticeably higher in the low fCO_2
399 mesocosms during Phases II and III (on average 80 %; Fig. 3d). Unfortunately, almost half of the
400 mortality assays in this second half of the experiment failed (see Materials and Methods), but the
401 successful assays suggest that losses were minor (<0.15 d^{-1}; Fig. 4d) and primarily due to grazing, as
402 no significant viral lysis was detected (Table S1).
403
404 **3.1.3 Nanoeukaryotes**
405 Nano-I showed maximum abundances (4.3 ± 0.4 x 10^2 ml^{-1}) on day 6 (except M1 which peaked on day
406 5), independent of fCO_2 (p=0.23, R^2=0.33; Fig. 3e). There was, however, a negative correlation of net
407 growth rate with fCO_2 during days 3-13 (NMDS-based period 1; p=0.01, R^2=0.79; Table 2, Fig. S2e). A
408 second major peak in abundance of Nano-I occurred on day 17, with markedly higher numbers in the
409 low fCO_2 mesocosms (4.1 x 10^2 ml^{-1} as compared to 2.4 x 10^2 ml^{-1} in high fCO_2 mesocosms; p=0.04,
410 R^2=0.67; Fig. 3e, Table 3 and Fig. S4g). Total loss rates in the high fCO_2 mesocosm M3 on days 6 and
411 10 were 2.3-fold higher compared to the low fCO_2 mescososm M1 (Fig. 4e), which may help to
412 explain this discrepancy in total abundance between low and high fCO_2 mesocosms. Viral lysis made
413 up to 98 % of total losses in the high fCO_2 mesocosm M3 during this period, whilst in M1 viral lysis
414 was only detected on day 13 (Table S1). Peak abundances (around 5.0 x 10^2 ml^{-1}) were much lower

compared to those in the surrounding waters (max ~2.4 x 10^3 ml^{-1}; Figs. 3e and S6a). During Phase II, Nano-I abundances in the surrounding waters displayed rather erratic dynamics compared to those of the mesocosms, but converged during certain periods (e.g. days 19-22). No significant relationship was found between net loss rates and fCO_2 for the second NMDS-based period ($p=0.26$, $R^2=0.30$; Table 2, Fig S.3e). At the end of Phase II, abundances were similar in all mesocosms but diverged again during Phase III (days 31-39) due primarily to a negative effect of CO_2 on Nano-I abundances, as depicted in the average 36 % reduction in Nano-I.

The temporal dynamics of Nano-II, the least abundant phytoplankton group analysed in our study, displayed the largest variability (Fig. 3f), perhaps due to the spread of this cluster in flow cytographs (which may indicate that this group represents several different phytoplankton species). No significant relationship was found between net growth rate and fCO_2 for this group for the two NMDS-based periods (Table 2, Figs S2f and S3f) nor with the peak in abundances on day 17 ($p=0.13$, $R^2=0.46$; Fig. S4h). Moreover, no consistent trend was detected in mortality rates (Fig. 4f). Similar to Nano-I, abundances in the surrounding water were often higher than in the mesocosms (max 3.5 x 10^2 ml^{-1} vs 1.1 x 10^4 ml^{-1}, respectively; Figs. 3f and S6b).

3.1.4 Algal carbon biomass

The mean combined biomass of Pico-I and Pico-II showed a strong positive correlation with fCO_2 throughout the experiment ($p<0.05$, $R^2=0.95$; Fig. 5a), an effect already noticeable by day 2. Their biomass in the high fCO_2 mesocosms was, on average 11 % higher than in the low fCO_2 mesocosms between days 10-20 and 20 % higher between days 20-39. Conversely, the remaining algal groups showed an average 10 % reduction in carbon biomass at enhanced fCO_2 (days 3-39, the sum of SYN, Pico-III, Nano-I and II ; $p<0.01$; Fig. 5b). The most notable response was found for the biomass of Pico-III, which showed an immediate negative response to CO_2 addition (Fig. S7a) and remained, on average, 29 % lower throughout the study period (days 2-39). For Nano-I and II the lower carbon biomass only became apparent during the end of Phase I and beginning of Phase II (days 14-20; Fig.

441 S7b). Due to its small cell size, the numerically dominant SYN accounted for an average of 40 % of
442 total carbon biomass.
443
444 **3.2 Prokaryote and virus population dynamics**
445 Prokaryote abundance in the mesocosms was positively related to total algal biomass independent of
446 treatment ($p<0.05$, $R^2=0.33$; Fig. 8) and generally followed total algal biomass (Fig. S7c). The initial
447 increase in total prokaryote abundances occurred during the first few days following the closure of
448 the mesocosms (Fig. 6a). This was primarily due to increases in the HNA-prokaryote group (Fig. 6b)
449 which displayed higher net growth rates (0.22 d^{-1}) compared to the LNA-prokaryotes (0.14 d^{-1} for
450 days -3 to 3; Fig. 6c). A similar, albeit somewhat lower, increase was also recorded in the surrounding
451 waters (Fig. 6a). The decline of the first peak in prokaryote abundances coincided with the decay in
452 phytoplankton abundance/biomass (Figs. 1a and S7c). Concurrently the share of viral lysis increased,
453 representing 37-39 % of total mortality on day 11 (Fig. 7b). No measurable rates of lysogeny were
454 found for the prokaryotic community during the experimental period (all phases). From days 10 to 15
455 prokaryote dynamics (total, HNA and LNA) became noticeably affected by CO_2 concentration with a
456 significant positive correlation between net growth and fCO_2 during Phase I (days 3-13 NMDS-based
457 period 1; Table 2, Fig. S2 g and h). In the higher fCO_2 mesocosms, the decline in prokaryote
458 abundance occurring between days 13 and 16 (Fig. 6a) was largely (70 %) due to decreasing HNA-
459 prokaryote numbers (Fig. 6b). The grazing was 1.6-fold higher in the high fCO_2 mesocosm M3
460 compared to M1 (0.36 ± 0.13 and 0.14 ± 0.08 d^{-1} on day 14; Fig. 7a). At the same time, virus
461 abundance increased in the high fCO_2 mesocosms (Fig. 6d).
462 During Phase II, prokaryote abundances increased steadily until day 24 (for both HNA and LNA),
463 corresponding to increased algal biomass (Figs. 6 and S7c) and lowered grazing rates (Fig. 7a).
464 Specifically, during days 16-24 (NMDS-based period 2), the HNA-prokaryotes showed an average 10
465 % higher abundances in the low, as compared to the high fCO_2 mesocosms (Fig. 6b). However, a
466 significant negative correlation of net growth rates and fCO_2 was only found for LNA (Table 2, Fig S3g

and h). No significant differences in loss rates between M1 and M3 were found during Phase II (p=0.22, 0.46 days 18 and 21 respectively; Fig. 7). Halfway through Phase II (day 24), the prokaryote abundance in the surrounding water leveled off (Fig. 6a). Prokaryote abundance ultimately declined during days 28-35 (Fig. 6a), whereby the net growth of LNA was again negatively correlated with enhanced CO_2 (p=0.02, R^2=0.76; Table 2, Fig S3g). Unfortunately, no experimental data on grazing and lysis of prokaryotes is present after day 25. However, viral abundances increased steadily at 2.2 x 10^6 d^{-1}, concomitant with a decline in prokaryote abundance (Fig. 6a and d). There was no significant correlation between viral abundances and fCO_2 during Phases II and III (p=0.36, R^2=0.21).

4 Discussion

In most experimental mesocosm studies, nutrients have been added to stimulate phytoplankton growth (Schulz et al., 2017) therefore little data exists for oligotrophic phytoplankton communities. In this study, we describe the impact of increased fCO_2 on the brackish Baltic Sea microbial community during summer (nutrient depleted; Paul et al., 2015). Small-sized phytoplankton numerically dominated the autotrophic community, in particular SYN and Pico-I (both about 1 µm cell diameter). Our results demonstrate variable effects of fCO_2 manipulation on temporal phytoplankton dynamics, dependent on phytoplankton group. In particular, Pico-I and Pico-II showed significant positive responses, whilst the abundances of Pico-III, SYN and Nano-I were negatively influenced by elevated fCO_2. The impact of OA on the different groups was, at times, a direct consequence of alterations in gross growth rate, whilst overall phytoplankton population dynamics could be explained by the combination of growth and losses. OA effects on community composition in these systems may have consequences on both the food web and biogeochemical cycling.

Comparison with surrounding waters

During Phase 0, the microbial assemblage showed good replicability between all mesocosms, however they had already began to deviate from the community in the surrounding waters. This was

493 most likely a consequence of water movement altering the physical conditions and biological
494 composition of the surrounding water body. The dynamic nature of water movement in this region
495 has been shown to alter the entire phytoplankton community several times over within a few
496 months, due to fluctuations in nutrient supply, advection, replacement/mixing of water masses and
497 water temperature (Lips and Lips, 2010). Alternatively, effects of enclosure and the techniques
498 (bubbling) used to ensure a homogenous water column may have stimulated SYN within the
499 mesocosms. By Phases II and III, the microbial abundances within the mesocosms were distinctly
500 different from the surrounding waters, with generally fewer SYN and Pico-I, and more Nano-I and
501 Nano-II. Our statistical analysis shows that during this time, there was little similarity between the
502 surrounding waters and mesocosms regardless of the CO_2 treatment level. Thus, the deviations
503 during this time were most likely due to an upwelling event in the archipelago (days 17-30; Paul et
504 al., 2015). Cold, nutrient-rich deep water has been shown to occur during summer, with profound
505 positive influence on ecosystem productivity (Nômmann et al., 1991; Lehman and Myrberg, 2008). A
506 relaxation from nutrient limitation in vertically stratified waters disproportionately favours larger-
507 sized phytoplankton, due to their higher nutrient requirements and lower capacity to compete at low
508 concentrations dictated by their lower surface to volume ratio (Raven, 1998; Veldhuis et al., 2005).
509 Inside the mesocosms, which were isolated from upwelled nutrients, picoeukaryotes dominated
510 similar to a stratified water column. Following this upwelling event, the pH of the surrounding
511 waters dropped from 8.3 to 7.8, a level comparable to the highest CO_2 treatment (M8) on day 32
512 (Paul et al., 2015). Suggesting that other factors contributed to the observed differences between
513 mesocosms and surrounding water, than can be accounted for by CO_2 concentration alone e.g.
514 nutrients. Alternatively, the magnitude and source of mortality occurring in the surrounding water
515 may have been altered, compared to within the mesocosms, after such an upwelling event. Although
516 the grazer community in the surrounding waters was not studied during this campaign, it is likely that
517 the grazing community was completely restructured during the upwelling event (Uitto et al., 1997). It
518 is nonetheless noteworthy that the phytoplankton groups with distinct responses to CO_2 enrichment

519 (either positive or negative) in the low (ambient) fCO_2 mesocosms diverged from those in the
520 surrounding water before the upwelling event occurred.
521
522 **Phytoplankton dynamics**
523 *Synechococcus* showed significantly lower net growth rates and peak abundances at higher fCO_2.
524 Both in laboratory and mesoscosm experiments, *Synechococcus* has been reported to have diverse
525 responses to CO_2, with approximately equal accounts of positive (Lu et al., 2006; Schulz et al., 2017),
526 negative (Paulino et al., 2007; Hopkins et al., 2010; Traving et al., 2014,) and insignificant changes (Fu
527 et al., 2007; Lu et al., 2006) in net growth rate with fCO_2. This variable response is probably due, at
528 least in part, to the broad physiological and genetic diversity of this species. In the Gulf of Finland
529 alone, 46 different strains of *Synechococcus* were isolated in July 2004 (Haverkamp et al. 2009).
530 Direct effects on physiology have been implied from laboratory studies. One isolate, a phycoerythrin
531 rich strain of *Synechococcus* WH7803 (Traving et al., 2014) elicited a negative physiological effect on
532 the growth rate from increased CO_2. This was most likely a consequence of higher sensitivity to the
533 lower pH (Traving et al., 2014), and the cellular cost of maintaining pH homeostasis or conversely a
534 direct effect on protein export. Additionally, Lu et al. (2006) reported increased growth rates in a
535 cultured phycocyanin rich but not a phycoerythrin rich strain of *Synechococcus*, suggesting that
536 pigments may play some part in defining the direct physiological response within *Synechococcus*. In
537 addition, within natural communities (Paulino et al., 2007; Hopkins et al., 2010; Schulz et al., 2017)
538 variability can also arise from indirect effects such a altering competition with other picoplankton
539 (Paulino et al., 2007). The delay and dampened effect of fCO_2 on SYN abundances within our study
540 was more likely due to indirect effects arising from alterations in food web dynamics than to direct
541 impacts on the physiology of this species. Specifically, significant differences in grazing rates of SYN
542 between M1 and M3 (days 10 and 17, no significant lysis detected) could be responsible for the
543 differing dynamics between the mesocosms at the end of Phase I and beginning of Phase II.

The gross growth rates of Pico-I were significantly higher ($p<0.05$) at high fCO_2 compared to the low CO_2 concentrations during the first 10 days of Phase I. Moreover, no differences were detected in the measured loss rates, demonstrating that increases in Pico-I were the due to increases in growth alone. The stimulation of Pico-I by elevated fCO_2 may be due to a stronger reliance on diffusive CO_2 entry compared to larger cells. Model simulations reveal that whilst near-cell CO_2/pH conditions are close to those of the bulk water for cells <5 µm in diameter, they diverge as cell diameters increase (Flynn et al., 2012). This is due to the size-dependent thickness of the diffusive boundary layer, which determines the diffusional transport across the boundary layer and to the cell surface (Wolf-Gladrow and Riebesell, 1997; Flynn et al., 2012). It is suggested that larger cells may be more able to cope with fCO_2 variability as their carbon acquisition is more geared towards handling low CO_2 concentrations in their diffusive boundary layer, e.g. by means of active carbon acquisition and bicarbonate utilization (Wolf-Gladrow and Riebesell, 1997; Flynn et al., 2012). Moreover, as the Baltic Sea experiences particularly large seasonal fluctuations in pH and fCO_2 (Jansson et al., 2013) due to the low buffering capacity of the waters, phytoplankton here are expected to have a higher degree of physiological plasticity. Our results agree with previous mesocosm studies, which reported enhanced abundances of picoeukaryotic phytoplankton (Brussaard et al., 2013; Davidson et al, 2016; Schulz et al., 2017), and particularly the prasinophyte *Micromonas pusilla* at higher fCO_2 (Engel et al., 2007; Meakin and Wyman, 2011). Furthermore, Schaum et al. (2012) found that 16 ecotypes of *Ostreococcus tauri* (another prasinophyte similar in size to Pico-I) increased in growth rate by 1.4-1.7 fold at 1,000 compared to 400 µatm fCO_2. All ecotypes increased their photosynthetic rates and those with most plasticity (those most able to vary their photosynthetic rate in response to changes in fCO_2) were more likely to increase in frequency within the community. It is possible that Pico-I cells are adapted to a highly variable carbonate system regime and are able to increase their photosynthetic rate when additional CO_2 is available. This ability would allow them to out-compete other phytoplankton (e.g. nanoeukaryotes in this study) in an environment when nutrients are scarce.

570 The net growth rates and peak abundances of Pico-II were also positively affected by fCO_2. Gross
571 growth rates were significantly higher at high fCO_2 on only two occasions (days 10 and 20) and were
572 accompanied by high total mortality rates. Pigment analysis suggests that both Pico-I and Pico-II are
573 chlorophytes (Paul et al., 2015) and as such may share a common evolutionary history (Schulz et al.,
574 2017); thus Pico-II may be stimulated by fCO_2 in a similar manner to Pico I. Chlorophytes are found in
575 high numbers at this site throughout the year (Kuosa, 1991), suggesting the ecological relevance of
576 Pico-I and Pico-II in this ecosystem. In addition, Pico-II bloomed exactly when Pico-I declined which
577 may suggest potential competitive exclusion.
578 Pico-III showed the most distinct and immediate response to CO_2 addition. The significant reduction
579 in gross growth rates observed during Phase I suggests a direct negative effect of CO_2 on the
580 physiology of these cells. For this group, the lower gross growth rates were matched by lower total
581 mortality rates with increased fCO_2. Although the mean cell size of Pico-III and Pico-II were
582 comparable (2.9 and 2.5 µm, respectively), they showed opposing responses to fCO_2 enrichment
583 (lower Pico-III abundances at high fCO_2). These differences may arise from taxonomic differences
584 between the two groups. Pico-III displayed relatively high phycoerythrin orange autofluorescence,
585 likely representing small-sized cryptophytes (Klaveness, 1989), although rod-shaped *Synechococcus*
586 up to 2.9 µm in length (isolated from this region; Haverkamp et al., 2009) or *Synechococcus*
587 microcolonies (often only two cells in the Baltic; Motwani and Gorokhove, 2013) cannot be excluded.
588 In agreement with Pico-III response to CO_2 enrichment, Hopkins et al. (2010) reported reduced
589 abundances of small cryptophytes under increased CO_2 in a mesocosm study in a Norwegian fjord
590 near Bergen.
591 Lastly, the two nanoeukaryotic phytoplankton groups also displayed a negative response to fCO_2
592 enrichment, whereby Nano-II was the least defined, most likely due to a high taxonomic diversity in
593 this group. Nano-I started to display lower abundances at high fCO_2 during Phase I (after day 10),
594 which was likely the result of greater differences between gross growth and total mortality
595 (compared to low fCO_2). Alternatively, enhanced nutrient competition due to increased abundances

596 of SYN and Pico-I (and later on also Pico-II) at elevated fCO_2 may also have contributed to the
597 dampened response of Nano-I in the high fCO_2 mesocosms. The overall decline in Nano-I, during
598 Phase II, and sustained low abundances during Phase III may well have been the result of grazing by
599 the increased mesozooplankton abundances during Phase II (Lischka et al., 2017).
600
601 **Microbial loop**
602 The strong association of prokaryote abundance with algal biomass, present throughout the
603 experiment, suggests that the effect of CO_2 was an indirect consequence of alterations in the
604 availability of phytoplankton carbon. Others have reported a tight coupling of autotrophic and
605 heterotrophic communities at this location, with an estimated 35 % of the total net primary
606 production being utilized directly by bacteria or heterotrophic flagellates (Kuosa and Kivi, 1989),
607 suggesting a highly efficient microbial loop in this ecosystem. In addition to phytoplankton exudation,
608 viral lysis may also contribute to the dissolved organic carbon pool (Wilhelm and Suttle, 1999;
609 Brussaard et al., 2005; Lønborg et al., 2013). We calculated that viral lysis of phytoplankton between
610 days 9 and 13 resulted in the release of 1.3 and 13.1 ng C ml^{-1} for M1 and M3, respectively. Assuming
611 a bacterial growth efficiency of 30 % and cellular carbon conversion of 7 fg C $cell^{-1}$ (Hornick et al.,
612 2017), we estimate that the organic carbon required to support bacterial dynamics during this period
613 (taking into account the net growth and loss rates) was 2.9 and 11.5 ng C ml^{-1} in low and high fCO_2
614 mesocosms M1 and M3, respectively. These results suggest that viral lysis of phytoplankton was an
615 important source of organic carbon for the bacterial community. Our results are consistent with
616 bacterial-phytoplankton coupling during this eastern Baltic Sea mesocosm study (Hornick et al.,
617 2017), and agree with earlier work on summer carbon flow in the northern Baltic Sea showing that
618 prokaryotic growth was largely supported by recycled carbon (Uitto et al., 1997). The average net
619 growth rates of the prokaryotes during the first period of increase in Phases 0 and I (0.2 d^{-1}) were
620 comparable to rates reported for this region (Kuosa, 1991). In order to sustain the concomitant daily
621 mortality (between 0.3-0.5 d^{-1}) measured during our study, prokaryotic gross growth rates must have

622 been close to one doubling a day (0.5-0.7 d^{-1}). During Phase I, grazing was the dominant loss factor of
623 the prokaryotic community although there was also evidence that viral lysis was occurring.
624 Bermúdez et al. (2016) reported the highest biomass of protozoans around day 15. This was
625 predominantly the heterotrophic choanoflagellate *Calliacantha natans,* which selectively feeds on
626 particles <1 µm in diameter (Marchant and Scott, 1993; Hornick et al., 2017). Indeed, an earlier study
627 in this area showed that heterotrophic nanoflagellates were the dominant grazers of bacteria,
628 responsible for ingestion of approximately 53 % of bacterial production compared to only 11 % being
629 grazing by ciliates (Uitto et al., 1997). During the first half of Phase II, grazing was reduced and likely
630 contributed to the steady increase in prokaryote abundances. Specifically, a negative relationship
631 between the abundances of HNA-prokaryotes and fCO_2 was detected and corresponded to reduced
632 bacterial production and respiration at higher fCO_2 (Hornick et al., 2017; Spilling et al., 2016).
633 Although CO_2 enrichment may not directly affect bacterial growth, co-occurring global rise in
634 temperature can increase enzyme activities, affecting bacterial production and respiration rates
635 (Piontek et al., 2009; Wohlers et al., 2009; Wohlers-Zöllner et al., 2011). Enhanced bacterial re-
636 mineralization of organic matter may stimulate autotrophic production by the small-sized
637 phytoplankton (Riebesell et al., 2009; Riebesell and Tortell, 2011; Engel et al., 2013), intensifying the
638 selection of small cell size.
639 Mean viral abundances were higher under CO_2 enrichment towards the end of Phase I and into Phase
640 II which is expected under conditions of increased phytoplankton and prokaryote biomass. The
641 estimated average viral burst size, obtained from this increase in total viral abundance and
642 concurrent decline in bacterial abundances, was about 30 which is comparable to published values
643 (Parada et al, 2006; Wommack and Colwell, 2000). Viral lysis rates of prokaryotes were measured
644 until day 25 and indicated that during days 18-25 an average 10-15 % of the total prokaryote
645 population was lysed per day. Moreover, the concurrent steady increase in viral abundances during
646 Phase III indicates that viral lysis of the prokaryotes remained important. Thus, the combined impact
647 of increased viral mortality together with reduced production (Hornick et al., 2017) ultimately led to

the decline in prokaryote abundance (this study). Lysogeny did not appear to be an important life strategy of viruses during our campaign. Direct effects of higher fCO_2 on viruses are not expected, as marine virus isolates are quite stable (both in terms of particle decay and loss of infectivity) over the range of pH of the present study (Danovaro et al., 2011; Mojica and Brussaard, 2014). The few studies which have inferred viral lysis rates based on changes in viral abundances show reduced abundances of algal viruses (e.g. *Emiliania huxleyi* virus) under enhanced CO_2 (Larsen et al., 2008) while mesocosm results by Brussaard et al. (2013) indicated a stronger impact of viruses on bacterial abundance dynamics with CO_2 enrichment.

5 Conclusions

Due to the low buffering capacity of the Baltic Sea and the paucity of data regarding OA impact in nutrient-limited waters, the results presented here are pertinent to increasing our understanding of how predicted rises in fCO_2 will affect the microbial communities in this region. Our study provides evidence that cell size, taxonomy and sensitivity to loss can all play a role in the outcome of CO_2 enrichment. Physiological constraints of cell size favour nutrient uptake by small cells under conditions of reduced nutrients and our results show that these effects can be further exacerbated by OA. Gross growth rates along with the complementary mortality rates allowed for a more comprehensive understanding of the phytoplankton population dynamics and thus perception of how microbial food web dynamics can influence the response of the autotrophic and heterotrophic components of the community. Our results further suggest that alterations in CO_2 concentrations are expected to affect prokaryote communities (mainly) indirectly through alterations in phytoplankton biomass, productivity and viral lysis. Overall, the combination of growth and losses (grazing and viral lysis) could explain microbial population dynamics observed in this study. It is noteworthy to mention, a recent study in the oligotrophic northeast Atlantic Ocean reported a shift from grazing-dominated to viral lysis-dominated phytoplankton community with strengthening of vertical stratification (shoaling the mixed layer depth and enhancing nutrient limitation) (Mojica et al., 2016).

Thus, we highly recommend that future research on OA combine mesocosm studies focusing on changes in microbial community composition and activity with experiments aimed at understanding the effects of OA on food web dynamics, i.e. partitioning mortality between grazing and viral lysis (Brussaard et al., 2008).

Author Contribution

Design and overall coordination of research by CB. Organization and performance of analyses in the field by KC. Data analysis by KC, CB, and SA-F. Design and coordination of the overall KOSMOS mesocosm project by UR. All authors contributed to the writing of the paper (KC, KM and CB are lead authors).

Acknowledgements

This project was funded through grants to C.B. by the Darwin project, the Netherlands Institute for Sea Research (NIOZ), and the EU project MESOAQUA (grant agreement number 228224). We thank the KOSMOS project organisers and team, in particular Andrea Ludwig, the staff of the Tvärminne Zoological Station and the diving team. We give special thanks to Anna Noordeloos, Kirsten Kooijman and Richard Doggen for their technical assistance during this campaign. We also gratefully acknowledge the captain and crew of R/V ALKOR for their work transporting, deploying and recovering the mesocosms. The collaborative mesocosm campaign was funded by BMBF projects BIOACID II (FKZ 03F06550) and SOPRAN Phase II (FKZ 03F0611).

References

Aberle, N., Schulz, K., Stuhr, A., Malzahn, A., Ludwig, A. and Riebesell, U.: High tolerance of microzooplankton to ocean acidification in an Arctic coastal plankton community, Biogeosciences, 10, 1471–1481, doi:10.5194/bg-10-1471-2013, 2013.

Barcelos e Ramos, J., Biswas, H., Schulz, K. G., LaRoche, J. and Riebesell, U.: Effect of rising atmospheric carbon dioxide on the marine nitrogen fixer *Trichodesmium*, Global Biogeochem. Cycles, 21(2), doi:10.1029/2006GB002898, 2007.

Baudoux, A. C., Noordeloos, A. A. M., Veldhuis, M. J. W. and Brussaard, C. P. D.: Virally induced mortality of *Phaeocystis globosa* during two spring blooms in temperate coastal waters, Aquat. Microb. Ecol., 44(3), 207–217, doi:10.3354/ame044207, 2006.

Bermúdez, J., Winder, M., Stuhr, A., Almén, A., Engström-Öst, J. and Riebesell, U.: Effect of ocean acidification on the structure and fatty acid composition of a natural plankton community in the Baltic Sea, Biogeosciences, 13, 6625–6635, doi:10.5194/bg- 13-6625-2016, 2016

Brussaard, C. P. D.: Optimization of Procedures for Counting Viruses by Flow Cytometry, Appl. Environ. Microbiol., 70(3), 1506–1513, doi:10.1128/AEM.70.3.1506-1513.2004, 2004.

Brussaard, C. P. D., Kuipers, B. and Veldhuis, M. J. W.: A mesocosm study of *Phaeocystis globosa* population dynamics: I. Regulatory role of viruses in bloom control, Harmful Algae, 4(5), 859–874, doi:10.1016/j.hal.2004.12.015, 2005.

Brussaard, C. P. D., Wilhelm, S. W., Thingstad, F., Weinbauer, M. G., Bratbak, G., Heldal, M., Kimmance, S. A., Middelboe, M., Nagasaki, K., Paul, J. H., Schroeder, D. C., Suttle, C. A., Vaqué, D. and Wommack, K. E.: Global-scale processes with a nanoscale drive: the role of marine viruses., ISME J., 2(6), 575–578, doi:10.1038/ismej.2008.31, 2008.

Brussaard, C. P. D., Noordeloos, A. A. M., Witte, H., Collenteur, M. C. J., Schulz, K., Ludwig, A. and Riebesell, U.: Arctic microbial community dynamics influenced by elevated CO_2 levels, Biogeosciences, 10, 719–731, doi:10.5194/bg-10-719-2013, 2013.

Clarke, K.R.: Non-parametric multivariate analyses of changes in community structure. Aust. J. Ecol., 18, 117-143, 1993.

Corno, G., Karl, D., Church, M., Letelier, R., Lukas, R., Bidigare, R. and Abbott, M.: Impact of climate forcing on ecosystem processes in the North Pacific Subtropical Gyre, J. Geophys. Res., 112, 1-14, 2007.

Danovaro, R., Corinaldesi, C., Dell'Anno, A., Fuhrman, J. A., Middelburg, J. J., Noble, R. T. and Suttle, C. A.: Marine viruses and global climate change, FEMS Microbiol. Rev., 35, 993–1034, 2011.

Davidson, A., McKinlay, J., Westwood, K., Thomson, P., Van Den Enden, R., De Salas, M., Wright, S., Johnson, R. and Berry, K.: Enhanced CO_2 concentrations change the structure of Antarctic marine microbial communities, Mar. Ecol. Progr. Ser., 552, 93–113. doi: 10.3354/meps11742, 2016.

Doney, S. C., Fabry, V. J., Feely, R. A. and Kleypas, J. A.: Ocean acidification: The other CO_2 problem, Annu. Rev. Mar. Sci., 1, 169–192, 2009.

Dutkiewicz, S., Morris, J.J., Follows, M.J., Scott, J., Levitan, O., Dyhrman, S.T., and Berman-Frank, I.: Impact of ocean acidification on the structure of future phytoplankton communities, Nat. Clim. Change, 5(11), 1002-1006, 2015.

Eberlein, T., Wohlrab, S., Rost, B., John, U., Bach, L. T., Riebesell, U. and Van de Waal, D. B.: Effects of ocean acidification on primary production in a coastal North Sea phytoplankton community, PLoS ONE, 12 (3). e0172594. DOI 10.1371/journal.pone.0172594, 2017.

Engel, A., Schulz, K., Riebesell, U., Bellerby, R., Delille, B. and Schartau, M.: Effects of CO_2 on particle size distribution and phytoplankton abundance during a mesocosm bloom experiment (PeECE II), Biogeosciences, 5, 509–521, doi:10.5194/bgd-4-4101-2007, 2007.

Engel, A., Borchard, C., Piontek, J., Schulz, K. G., Riebesell, U. and Bellerby, R.: CO_2 increases ^{14}C primary production in an Arctic plankton community, Biogeosciences, 10(3), 1291–1308, doi:10.5194/bg-10-1291-2013, 2013.

Evans, C. and Brussaard, C.P.D.: Regional variation in lytic and lysogenic viral infection in the Southern Ocean and its contribution to biogeochemical cycling. Appl. Environ. Microbiol.,78 (18), 6741-6748, 2012.

Feng, Y., Leblanc, K., Rose, J. M., Hare, C. E., Zhang, Y., Lee, P. A., Wilhelm, S. W., DiTullio, G. R., Rowe, J. M., Sun, J., Nemcek, N., Gueguen, C., Passow, U., Benner, I., Hutchins, D. A. and Brown, C.: Effects of increased pCO_2 and temperature on the North Atlantic spring bloom. I. The phytoplankton community and biogeochemical response, Mar. Ecol. Progr. Ser., 388, 13–25, doi: 10.3354/meps08133, 2009.

Field, C. B., Behrenfeld, M. J., Randerson, J. T. and Falkowski, P.: Primary Production of the Biosphere: Integrating Terrestrial and Oceanic Components, Science, 281(5374), 237–240, doi:10.1126/science.281.5374.237, 1998.

Flynn, K. J., Blackford, J. C., Baird, M. E., Raven, J. A., Clark, D. R., Beardall, J., Brownlee, C., Fabian, H. and Wheeler, G. L.: Letter. Changes in pH at the exterior surface of plankton with ocean acidification, Nat. Clim. Change, 2(7), 510–513, doi:10.1038/nclimate1696, 2012.

Fu, F. X., Warner, M. E., Zhang, Y., Feng, Y. and Hutchins, D. A.: Effects of increased temperature and CO_2 on photosynthesis, growth, and elemental ratios in marine *Synechococcus* and *Prochlorococcus* (Cyanobacteria), J. Phycol., 43(3), 485–496, doi:10.1111/j.1529-8817.2007.00355.x, 2007.

Garrison, D. L., Gowing, M. M., Hughes, M. P., Campbell, L., Caron, D. A., Dennett, M. R., Shalapyonok, A., Olson, J. A., Landry, M. R., Brown, S. L., Liu, H-B., Azam, F., Steward, G. F., Ducklow, H. W. and Smith, D. C.: Microbial food web structure in the Arabian Sea: A US JGOFS study. Deep-Sea Res.Part II, 47, 1387-1422, doi:10.1016/S0967-0645(99)001 48-4, 2000.

Gruber, N.: Warming up, turning sour, losing breath: Ocean biogeochemistry under global change, Phil. Trans. R. Soc. A, 369, 1980–1996, 2011.

Haverkamp, T., Schouten, D., Doeleman, M., Wollenzien, U., Huisman, J. and Stal, L.: Colorful microdiversity of *Synechococcus* strains (picocyanobacteria) isolated from the Baltic Sea, ISME J., 3, 397−408, 2009.

Hein, M. and Sand-Jensen, K.: CO_2 increases oceanic primary production, Nature, 388(6642), 526–527, 1997.

Hopkins, F. E., Turner, S. M., Nightingale, P. D., Steinke, M., Bakker, D., and Liss, P. S.: Ocean acidification and marine trace gas emissions, P. Natl. Acad. Sci. USA, 107, 760–765, doi:10.1073/pnas.0907163107, 2010.

Hornick, T., Bach, L. T., Crawfurd, K. J., Spilling, K., Achterberg, E. P., Brussaard, C. P. D., Riebesell, U., and Grossart, H.-P.:Ocean acidification indirectly alters trophic interaction of heterotrophic bacteria at low nutrient conditions, Biogeosciences, 14, 1-15, doi:10.5194/bg-2016-61, 2017.

Hutchins, D. A., Fe, F-X., Zhang, Y., Warner, M. E., Feng, Y., Portune, K., Bernhardt, P.W. and Mulholland, M.R.: CO_2 control of *Trichodesmium* N_2 fixation, photosynthesis, growth rates, and elemental ratios: implications for past, present, and future ocean biogeochemistry, Limnol. Oceanogr., 52(4), 1293–1304, 2007.

Jansson, A., Norkko, J. and Norkko, A.: Effects of Reduced pH on *Macoma balthica* Larvae from a System with Naturally Fluctuating pH-Dynamics, PLoS One, 8(6), doi:10.1371/journal.pone.0068198, 2013.

Kimmance, S. A. and Brussaard, C. P. D.: Estimation of viral-induced phytoplankton mortality using the modified dilution method, in: Manual of Aquatic Viral Ecology, edited by: Wilhelm S. W., Weinbauer M., Suttle C. A., pp 65–73, ASLO, 2010.

Klaveness, D.: Biology and ecology of the Cryptophyceae: status and challenges., Biol Ocean., 6, 257–270, 1989.

Kulinski, K. and Pempkowiak, J.: The carbon budget of the Baltic Sea, Biogeosciences, 8, 4841–4869, 2011.

Kuosa, H.: Picoplanktonic algae in the northern Baltic Sea: seasonal dynamics and flagellate grazing, Mar. Ecol. Prog. Ser., 73(2-3), 269–276, doi:10.3354/meps073269, 1991.

Kuosa, H. and Kivi, K.: Bacteria and heterotrophic flagellates in the pelagic carbon cycle in the northern Baltic Sea, Mar. Ecol. Prog. Ser., 53, 93–100, doi:10.3354/meps053093, 1989.

Larsen, J. B., Larsen, A., Thyrhaug, R., Bratbak, G. and Sandaa, R. A.: Response of marine viral populations to a nutrient induced phytoplankton bloom at different pCO_2 levels, Biogeosciences, 5, 523–533, doi:10.5194/bg-5-523-2008, 2008.

Legendre, P., and Legendre, L.:Numerical Ecology. Amsterdam; New York: Elsevier, 1998.

Lehmann, A. and Myrberg, K.: Upwelling in the Baltic Sea – A review, J. Marine Syst., 74, S3–S12, doi:10.1016/j.jmarsys.2008.02.010, 2008.

Leonardos, N. and Geider, R. J.: Elevated atmospheric carbon dioxide increases organic carbon fixation by *Emiliania huxleyi* (Haptophyta), under nutrient-limited high-light conditions, J. Phycol., 41(6), 1196–1203, doi:0.1111/j.1529-8817.2005.00152.x, 2005.

Lips, I. and Lips, U.: Phytoplankton dynamics affected by the coastal upwelling events in the Gulf of Finland in July-August 2006. J. Plankton Res., 32 (9), 1269–1282, 2016.

Lischka, S., Bach, L.T., Schulz, K.G. and Riebesell, U.: Micro- and mesozooplankton community response to increasing levels of fCO_2 in the Baltic Sea: insights from a large-scale mesocosm experiment, Biogeosciences, 14, 447-466, doi:10.5194/bg-14-447-2017, 2017.

Lønborg, C., Middelboe, M. and Brussaard, C. P. D.: Viral lysis of Micromonas pusilla: Impacts on dissolved organic matter production and composition, Biogeochemistry, 116(1-3), 231–240, doi:10.1007/s10533-013-9853-1, 2013.

Lu, Z., Jiao, N. and Zhang, H.: Physiological changes in marine picocyanobacterial *Synechococcus* strains exposed to elevated CO_2 partial pressure, Mar. Biol. Res., 2(6), 424–430, doi:10.1080/17451000601055419, 2006.

Marchant, H.J. and Scott F.J: Uptake of sub-micrometre particles and dissolved organic material by Antarctic choanoflagellates, Mar. Ecol. Prog. Ser., 92, 59-64, 1993.

Marie, D., Brussaard, C. P. D., Thyrhaug, R., Bratbak, G. and Vaulot, D.: Enumeration of marine viruses in culture and natural samples by flow cytometry, Appl. Environ. Microbiol., 65(1), 45–52, 1999.

Meakin, N. G. and Wyman, M.: Rapid shifts in picoeukaryote community structure in response to ocean acidification., ISME J., 5(9), 1397-405, doi:10.1038/ismej.2011.18, 2011.

Meyer, J. and Riebesell, U.: Reviews and Syntheses: Responses of coccolithophores to ocean acidification: a meta-analysis, Biogeosciences, 12(6), 1671–1682, doi:10.5194/bg-12-1671-2015, 2015.

Middelboe, M. and Lyck, P. G.: Regeneration of dissolved organic matter by viral lysis in marine microbial communities, Aquat. Microb. Ecol., 27(2), 187–194, doi:10.3354/ame027187, 2002.

Mojica, K. D. A., Evans, C. and Brussaard, C. P. D.: Flow cytometric enumeration of marine viral populations at low abundances, Aquat. Microb. Ecol., 71(3), 203–209, doi:10.3354/ame01672, 2014.

Mojica, K. D. A. and Brussaard, C. P. D.: Factors affecting virus dynamics and microbial host–virus interactions in marine environments, FEMS Microbiol. Ecol., 89(3), 495–515, doi:10.1111/1574-6941.12343, 2014.

Mojica, K. D. A., Huisman, J., Wilhelm, S. W. and Brussaard, C. P. D.: Latitudinal variation in virus-induced mortality of phytoplankton across the North Atlantic Ocean, ISME J., doi:10.1038/ismej.2015.130, 2016.

Motwani, N., and Gorokhova, E.: Mesozooplankton grazing on picocyanobacteria in the Baltic Sea as inferred from molecular diet analysis, PLoS ONE, 8: e79230, 2013.

Niehoff, B., Schmithüsen, T., Knüppel, N., Daase, M., Czerny, J., and Boxhammer, T.: Mesozooplankton community development at elevated CO_2 concentrations: results from a mesocosm experiment in an Arctic fjord, Biogeosciences, 10, 1391–1406, doi:10.5194/bg-10-1391-2013, 2013.

Nõmmann, S., Sildam, J., Nõges, T. and Kahru, M.: Plankton distribution during a coastal upwelling event off Hiiumaa, Baltic Sea: impact of short-term flow field variability. Cont. Shelf Res., 11 (1), 95-108, 1991.

Oksanen, J., Blanchet, F. G., Friendly, M., Kindt, R., Legendre, P., McGlinn, D., Minchin, P., R., O'Hara, R. B., L. Simpson, G. L., Solymos, P., Stevens, M. H. H., Szoecs, E. and Wagner, H.: vegan: Community Ecology Package. R package version 2.4-3. https://CRAN.R-project.org/package=vegan, 2017.

Parada, V., Herndl, G. and Weinbauer, M.:Viral burst size of heterotrophic prokaryotes in aquatic systems. J. Mar. Biol. Assoc. U. K., 86, 613-621, doi:10.1017/S002531540601352X, 2006.

Paul, A. J., Bach, L. T., Boxhammer, T., Czerny, J., Hellemann, D., Trense, Y., Nausch, M., Sswat, M., Riebesell, U., Road, M., Lismore, E. and Way, E.: Effect of elevated CO_2 on organic matter pools and fluxes in a summer , post spring-bloom Baltic Sea plankton community, Biogeosciences, 12, 6181–6203, doi: 10.5194/bg-12-6181-2015, 2015.

Paulino, A. I., Egge, J. K. and Larsen, A.: Effects of increased atmospheric CO_2 on small and intermediate sized osmotrophs during a nutrient induced phytoplankton bloom, Biogeosciences Discuss., 4(6), 4173–4195, doi:10.5194/bgd-4-4173-2007, 2007.

Pfeil, B., Olsen, A., Bakker, D. C. E., Hankin, S., Koyuk, H., Kozyr, A., Malczyk, J., Manke, A., Metzl, N., Sabine, C. L., Akl, J., Alin, S. R., Bates, N., Bellerby, R. G. J., Borges, A., Boutin, J., Brown, P. J., Cai, W. J., Chavez, F. P., Chen, A., Cosca, C., Fassbender, A. J., Feely, R. A., González-Dávila, M., Goyet, C., Hales, B., Hardman-Mountford, N., Heinze, C., Hood, M., Hoppema, M., Hunt, C. W., Hydes, D., Ishii, M., Johannessen, T., Jones, S. D., Key, R. M., Körtzinger, A., Landschützer, P., Lauvset, S. K., Lefèvre, N., Lenton, A., Lourantou, A., Merlivat, L., Midorikawa, T., Mintrop, L., Miyazaki, C., Murata, A., Nakadate, A., Nakano, Y., Nakaoka, S., Nojiri, Y., Omar, A. M., Padin, X. A., Park, G. H., Paterson, K., Perez, F. F., Pierrot, D., Poisson, A., Ríos, A. F., Santana-Casiano, J. M., Salisbury, J., Sarma, V. V. S. S., Schlitzer, R. , Schneider, B. , Schuster, U. , Sieger, R. , Skjelvan, I. , Steinhoff, T. , Suzuki, T. , Takahashi, T. , Tedesco, K. , Telszewski, M. , Thomas, H. , Tilbrook, B. , Tjiputra, J. , Vandemark, D. , Veness, T. , Wanninkhof, R. , Watson, A. , Weiss, R. , Wong, C. and Yoshikawa-Inoue, H.: A uniform, quality controlled Surface Ocean CO_2 Atlas (SOCAT) , Earth Syst. Sci. Data Discuss., 5 (2), 735-780, doi: 10.5194/essdd-5-735-2012, 2012.

Pinheiro, J., Bates, D., DebRoy, S., Sarkar, D. and R Core Team.: nlme: Linear and Nonlinear Mixed Effects Models. R package version 3.1-131, https://CRAN.R project.org/package=nlme, 2017.

Piontek, J., Händel, N., Langer, G., Wohlers, J., Riebesell, U. and Engel, A.: Effects of rising temperature on the formation and microbial degradation of marine diatom aggregates, Aquat. Microb. Ecol., 54, 305–318, doi:10.3354/ame01273, 2009.

Qiu, B. and Gao, K.: Effects of CO_2 enrichment on the bloom-forming cyanobacterium *Microcystis aeruginosa* (Cyanophyceae): Physiological responses and relationships with the availability of dissolved inorganic carbon, J. Phycol., 38(4), 721–729, doi:10.1046/j.1529-8817.2002.01180.x, 2002.

R Core Team, R: A language and environment for statistical computing. R Foundation for Statistical Computing, Vienna, Austria. URL https://www.R-project.org/, 2017.

Raven, J. A.: The twelfth Tansley Lecture. Small is beautiful: The picophytoplankton, Funct. Ecol., doi:10.1046/j.1365-2435.1998.00233.x, 1998.

Riebesell, U., Körtzinger, A. and Oschlies, A.: Sensitivities of marine carbon fluxes to ocean change, Proc. Natl. Acad. Sci. U. S. A., 106(49), 20602–20609, doi:10.1073/pnas.0813291106, 2009.

Riebesell, U. and Tortell, P. D.: Effects of ocean acidification on pelagic organisms and ecosystems, in: Ocean Acidification, edited by: Gattuso, J.-P. and Hansson, L., p. 99, Oxford University Press, Oxford, United Kingdom, 2011.

Riebesell, U., Czerny, J., von Bröckel, K., Boxhammer, T., Büdenbender, J., Deckelnick, M., Fischer, M., Hoffmann, D., Krug, S.A., Lentz, U., Ludwig, A., Muche, R. and Schulz, K. G.: Technical Note: A mobile sea-going mesocosm system – new opportunities for ocean change research, Biogeosciences, 10, 1835–1847, doi:10.5194/bg-10-1835-2013, 2013.

Riebesell, U., Bach, L. T., Bellerby, R. G. J., Bermudez, R., Boxhammer, T., Czerny, J., Larsen, A., Ludwig, A. and Schulz, K. G.: Ocean acidification impairs competitive fitness of a predominant pelagic calcifier, Nature Geoscience, 10, 19-24, doi:10.1038/ngeo2854, 2017.

Rose, J. M., Feng, Y., Gobler, C. J., Gutierrez, R., Harel, C. E., Leblancl, K. and Hutchins, D. A.: Effects of increased pCO_2 and temperature on the North Atlantic spring bloom. II. Microzooplankton abundance and grazing, Mar. Ecol. Prog. Ser., 388, 27–40, doi:10.3354/meps08134, 2009.

Schaum, E., Rost, B., Millar, A. J. and Collins, S.: Variation in plastic responses of a globally distributed picoplankton species to ocean acidification, Nat. Clim. Change, 3, 298–302. doi: 10.1038/nclimate1774, 2012.

Schulz, K. G. and Riebesell, U.: Diurnal changes in seawater carbonate chemistry speciation at increasing atmospheric carbon dioxide, Mar. Biol., 160, 1889–1899, doi:10.1007/s00227-012-1965-y, 2013.

Schulz, K., Bach, L., Bellerby, R., Bermúdez, R., Büdenbender, J., Boxhammer, T., Czerny, J., Engel, A., Ludwig, A., Meyerhöfer, M., Larsen,A., Paul, A., Sswat, M.l., Riebesell, U.: Phytoplankton Blooms at Increasing Levels of Atmospheric Carbon Dioxide: Experimental Evidence for Negative Effects on Prymnesiophytes and Positive on Small Picoeukaryotes, Frontiers in Marine Science, 4, 64 , 2017.

Sheik, A. R., Brussaard, C. P. D., Lavik, G., Lam, P., Musat, N., Krupke, A., Littmann, S., Strous, M. and Kuypers, M. M. M.: Responses of the coastal bacterial community to viral infection of the algae Phaeocystis globosa, ISME J., 8(1), 212–25, doi:10.1038/ismej.2013.135, 2014.

Sherr, E.B., Caron, D. A. and B. F. Sherr.: Staining of heterotrophic protists for visualization via epifluorescence microscopy, in: Current Methods in Aquatic Microbial Ecology, edited by: B. Sherr, E. Sherr and J. C. P. Kemp, pp. 213–228, Lewis Publ., N.Y., 1993.

Spilling, K., Paul, A. J., Virkkala, N., Hastings, T., Lischka, S., Stuhr, A., Bermudez, R., Czerny, J., Schulz, K. G., Ludwig, A. and Riebesell, U.: Ocean acidification decreases plankton respiration: evidence from a mesocosm experiment , Biogeosciences, 13, 4707-4719, 2016.

Stoecker, D. K., Nejstgaard, J., Madhusoodhanan, R. and Larsen, A.: Underestimation of microzooplankton grazing in dilution experiments due to inhibition of phytoplankton growth, Limnol. Oceanogr., 60, 1426–1438, doi:10.1002/lno.10106, 2015.

Suffrian, K., Simonelli, P., Nejstgaard, J. C., Putzeys, S., Carotenuto, Y. and Antia, A. N.: Microzooplankton grazing and phytoplankton growth in marine mesocosms with increased CO_2 levels, Biogeosciences, 5, 1145–1156, 2008.

Tortell, P. D., DiTullio, G. R., Sigman, D. M. and Morel, F. M. M.: CO_2 effects on taxonomic composition and nutrient utilization in an Equatorial Pacific phytoplankton assemblage, Mar. Ecol. Prog. Ser., 236, 37–43, 2002.

Traving, S. J., Clokie, M. R. J. and Middelboe, M.: Increased acidification has a profound effect on the interactions between the cyanobacterium Synechococcus sp. WH7803 and its viruses, FEMS Microbiol. Ecol., 87(1), 133–141, doi:10.1111/1574-6941.12199, 2014.

Turley, C. and Boot, K.: UNEP emerging issues: Environmental consequences of ocean acidification: A threat to food security, United Nations Environ. Program., 2010.

Uitto, A., Heiskanen, A., Lignell, R., Autio, R., and Pajuniemi, R.: Summer dynamics of the coastal planktonic food web in the northern Baltic Sea, Mar. Ecol. Prog. Ser., 151, 27–41, doi:10.3354/meps151027, 1997.

Veldhuis, M. J. W. and Kraay, G. W.: Phytoplankton in the subtropical Atlantic Ocean: Towards a better assessment of biomass and composition, Deep. Res. Part I Oceanogr. Res. Pap., 51(4), 507–530, doi:10.1016/j.dsr.2003.12.002, 2004.

Veldhuis, M. J. W., Timmermans, K. R., Croot, P. and Van Der Wagt, B.: Picophytoplankton; A comparative study of their biochemical composition and photosynthetic properties, J. Sea Res., 53(1-2 SPEC. ISS.), 7–24, doi:10.1016/j.seares.2004.01.006, 2005.

Weinbauer, M. G.: Ecology of prokaryotic viruses, FEMS Microbiol. Rev., 28(2), 127–181, doi:10.1016/j.femsre.2003.08.001, 2004.

Weinbauer, M. G. and Suttle, C. A.: Potential significance of lysogeny to bacteriophage production and bacterial mortality in coastal waters of the Gulf of Mexico, Appl. Environ. Microbiol., 62(12), 4374–4380, 1996.

Weinbauer, M. G., Mari, X. and Gattuso, J.-P.: Effect of ocean acidification on the diversity and activity of heterotrophic marine microorganisms, in: Ocean Acidification, edited by: Gattuso, J.-P. and Hansson, L., p. 83-98, Oxford University Press, Oxford, United Kingdom, 2011.

Wilhelm, S. W. and Suttle, C. A.: Viruses and Nutrient Cycles in the Sea aquatic food webs, Bioscience, 49(10), 781–788, doi:10.2307/1313569, 1999.

Wilhelm, S. W., Brigden, S. M. and Suttle, C. A.: A dilution technique for the direct measurement of viral production: A comparison in stratified and tidally mixed coastal waters, Microb. Ecol., 43(1), 168–173, doi:10.1007/s00248-001-1021-9, 2002.

Winget, D. M., Williamson, K. E., Helton, R. R. and Wommack, K. E.: Tangential flow diafiltration: An improved technique for estimation of virioplankton production, Aquat. Microb. Ecol., 41(3), 221–232, doi:10.3354/ame041221, 2005.

Wohlers, J., Engel, A., Zöllner, E., Breithaupt, P., Jürgens, K., Hoppe, H.-G., Sommer, U. and Riebesell, U.: Changes in biogenic carbon flow in response to sea surface warming., Proc. Natl. Acad. Sci. U. S. A., 106(17), 7067–7072, doi:10.1073/pnas.0812743106, 2009.

Wohlers-Zöllner, J., Breithaupt, P., Walther, K., Jürgens, K. and Riebesell, U.: Temperature and nutrient stoichiometry interactively modulate organic matter cycling in a pelagic algal-bacterial community, Limnol. Oceanogr., 56(2), 599–610, doi:10.4319/lo.2011.56.2.0599, 2011.

Wolf-Gladrow, D. and Riebesell, U.: Diffusion and reactions in the vicinity of plankton: A refined model for inorganic carbon transport, Mar. Chem., 59(1-2), 17–34, doi:10.1016/S0304-4203(97)00069-8, 1997.

Wommack, K.E. and Colwell, R.R.:Virioplankton: viruses in aquatic ecosystems, Microbiol. Mol. Biol. Rev., 64, 69–114, 2000.

Worden, A. Z., Nolan, J.,K., and Palenik, B.:Assessingthe dynamics and ecology of marine picophytoplankton: The importance of the eukaryotic component. Limnol.Oceanogr., 49, 168-179, doi:10.4319/lo.2004.49.1.0168, 2004.

Zuur, A. F., Ieno, E. N. and Smith, G. M.: Analysing Ecological Data, Springer New York, doi: 10.1007/978-0-387-45972-1, 2007.

Table 1. fCO_2 concentrations (µatm) averaged over the duration of the experiment (following CO_2 addition) and subsequent classification as low, intermediate or high. Mesocosms sampled for mortality assays are denoted by an asterisk. The symbols and colours are used throughout this manuscript and corresponding articles in this issue.

Mesocosm	***M1****	***M5***	***M7***	***M6***	***M3****	***M8***
CO_2 Level	***LOW***	***LOW***	***INTERMEDIATE***	***INTERMEDIATE***	***HIGH***	***HIGH***
Mean fCO_2 (µatm) days 1-43	***365***	***368***	***497***	***821***	***1007***	***1231***
Symbol						

Table 2. The fit (R^2) and significance (*p*-value) of linear regressions applied to assess the relationship between net growth rate and temporally averaged fCO_2 for the different microbial groups distinguished by flow cytometry. The results presented are for two periods distinguished from NMDS analysis; NMDS-based period 1 (days 3-13) and 2 (days 16-24). A significance level of p≤0.05 was taken and significant results are shown in bold.

Phytoplankton Group	***NMDS period 1 (days 3-13)***		***NMDS period 2 (days 16-24)***	
	p	***R^2***	***p***	***R^2***
SYN	*0.10*	*0.53*	***0.05***	***0.63***
Pico-I	***0.01***	***0.80***	***0.05***	***0.64***
Pico-II	*0.52*	*0.11*	*0.10*	*0.52*
Pico-III	***0.04***	***0.67***	***<0.01***	***0.91***
Nano-I	***0.01***	***0.79***	*0.26*	*0.30*
Nano-II	*0.20*	*0.36*	*0.06*	*0.61*
HNA	***0.05***	***0.64***	*0.89*	*0.00*
LNA	***<0.01***	***0.95***	***0.02***	***0.76***

Table 3. The fit (R^2) and significance (*p*-value) of linear regressions used to relate peak abundances and net growth rate with temporally averaged fCO_2 for the different microbial groups distinguished by flow cytometry during specific periods of interest. A significance level of p≤0.05 was taken and significant results are shown in bold.

	Peak abundance		***Net growth rate***	
	p	***R2***	***p***	***R2***
SYN day 24	***0.01***	***0.80***		
Pico-I day 5	***0.01***	***0.81***		
Pico-I day 13	***<0.01***	***0.94***		
Pico-I day 21	***0.01***	***0.84***		
Pico-II day 17	***<0.01***	***0.93***		
Pico-III day 24	***<0.01***	***0.91***		
Nano-I day 17	***0.04***	***0.67***		
Pico-I days 1-5			***<0.01***	***0.90***
Pico-I days 5-9			***<0.01***	***0.89***
Pico-II days 12-17			***0.01***	***0.82***

Figure captions

Fig. 1. (a) Time-series plot of depth-integrated (0.3–10 m) total phytoplankton abundance (< 20 µm) and **(b)** total eukaryotic phytoplankton abundance for each mesoscosm and the surrounding waters (Baltic). Dotted lines indicate the end of Phase I and end of Phase II. Colours and symbols represent the different mesocosms and are consistent throughout the manuscript. Mean fCO_2 during the experiment (days 1-43) were: M1, 365 µatm; M3, 1007 µatm; M5, 368 µatm; M6, 821 µatm; M7, 497 µatm; M8, 1231 µatm.

Fig. 2. Non-metric multidimensional scaling (NMDS) ordination plot of microbial community development in each mesocosm and surrounding waters (Baltic) over the experimental period. Phases are indicated by different open symbols. Days of experiment (DoE) when communities separate (3,13,16 and 24) are indicated by different closed symbols. Phytoplankton groups are denoted as: SYN (Syn), Pico-I (P-I), Pico-II (P-II), Pico-III (P-III), Nano-I (N-I), Nano-II (N-II), Low NA prokaryotes (LNA) and High NA prokaryotes (HNA).

Fig. 3. Time-series plot of depth-integrated (0.3–10 m) abundances of **(a)** *Synechococcus* (SYN) **(b)** picoeukaryotes I (Pico-I) **(C)** picoeukaryotes II (Pico-II) **(d)** picoeukaryotes III (Pico-III) **(e)** nanoeukaryotes I (Nano-I) and **(f)** nanoeukaryotes II (Nano-II) distinguished by flow cytometric analysis of the microbial community in each mesocosm and the surrounding waters (Baltic). Dotted lines indicate the end of Phase I and end of Phase II, grey areas indicate NMDS-based periods 1 and 2 where net growth rates were analysed.

Fig. 4. Total mortality rates (i.e., grazing and lysis, solid bars) and gross growth rates (striped bars) d^{-1} of the different phytoplankton groups in mesocosms M1 (blue) and M3 (red) on the day indicated: **(a)** *Synechococcus* (SYN) **(b)** picoeukaryotes I (Pico-I) **(C)** picoeukaryotes II (Pico-II) **(d)** picoeukaryotes III (Pico-III) **(e)** nanoeukaryotes I (Nano-I) and **(f)** nanoeukaryotes II (Nano-II). Significant ($p \leq 0.05$) differences between mesocosms are indicated by an asterisk above the relevant bar (either total loss or gross growth). A colored zero indicates that a rate of zero was measured in the mesocosm of the corresponding colour and the absence of a bar, or zero indicates a failed experiment. Dotted lines indicate the end of Phase I and end of Phase II.

Fig. 5. Time-series plot of the mean phytoplankton carbon biomass in high fCO_2 (M3,6,8; red) and low fCO_2 (M1,5,7; blue) mesocosms of **(a)** Pico I and II combined and **(b)** SYN, Pico III, Nano I and II

combined. Error bars represent one standard deviation from the mean. Carbon biomass calculated assuming a spherical diameter equivalent to the mean average cell diameters for each group and conversion factors of 237 fg C μm^{-3} (Worden et al.2004) and 196.5 fg C μm^{-3} (Garrison et al. 2000) for pico- and nano-sized plankton, respectively. Dotted lines indicate the end of Phase I and end of Phase II.

Fig. 6. Time series plot of depth-integrated (0.3–10 m) abundances of **(a)** Total prokaryotes **(b)** High fluorescent nucleic acid prokaryote population (HNA) **(c)** Low fluorescent nucleic acid prokaryote population (LNA) and **(d)** Total virus. Dotted lines indicate the end of Phase I and end of Phase II, grey areas indicate NMDS-based periods where net growth rates were analysed.

Fig. 7. Prokaryote mortality rates: **(a)** Total grazing (d^{-1}) and **(b)** viral lysis rates as % of prokaryote standing stock, in mesocosms M1 (low fCO_2, blue) and M3 (high fCO_2, red). Grazing rates were determined from fluorescently labelled prey, viral lysis rates from viral production assays. Error bars represent one standard deviation of triplicate assays. Significant ($p \leq 0.05$) differences between mesocosms are indicated by an asterisk. Dotted lines indicate the end of Phase I.

Fig. 8. Correlation between total carbon biomass ($\mu mol\ L^{-1}$) and total prokaryote abundance in low fCO_2 mesocosms (M1, 5 and 7; blue) and high fCO_2 mesocosms (M3,6, 8; red) throughout the experiment (days -2 to 39).

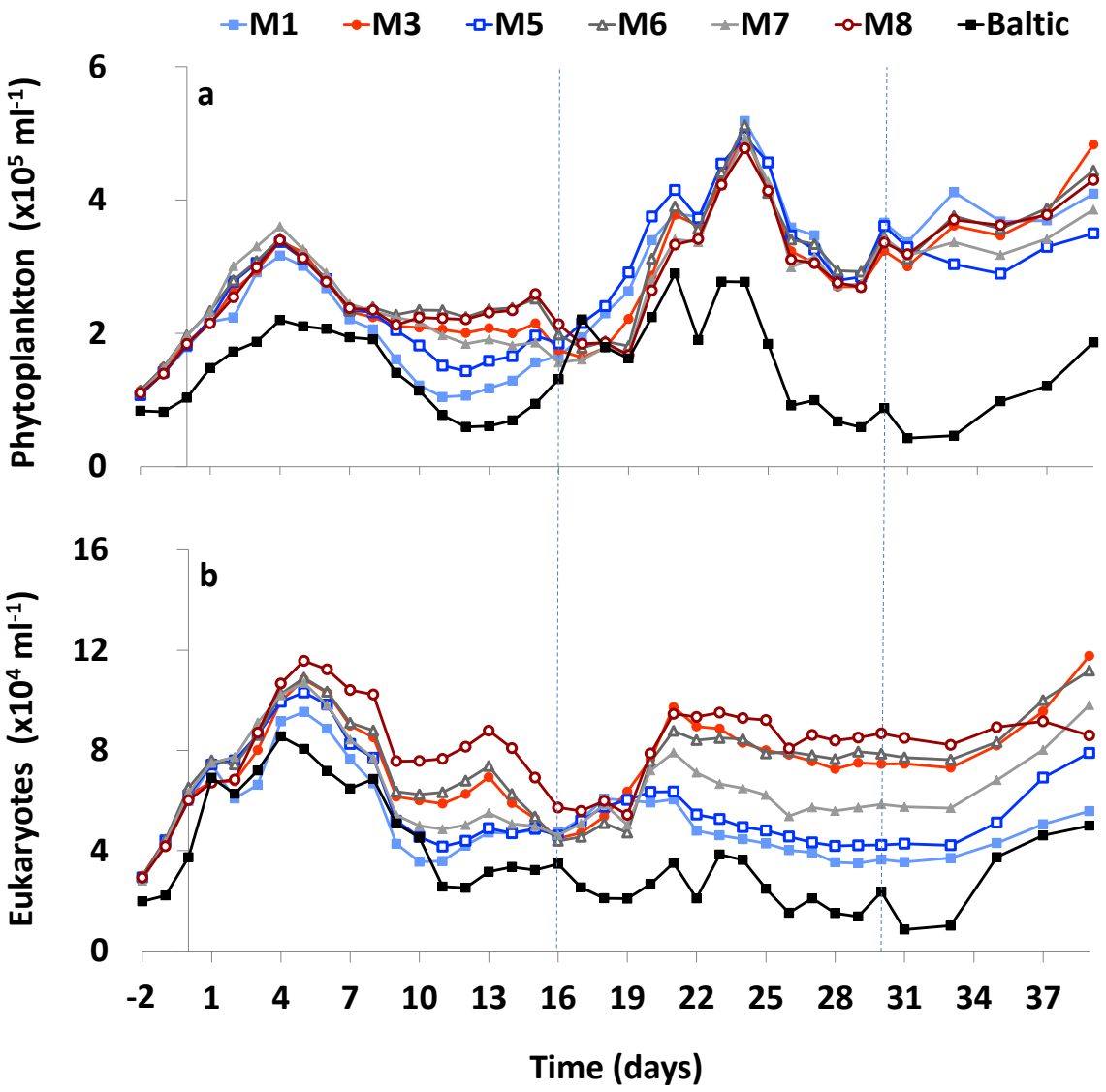
M1
M3
M5
M6
M7
M8
Baltic
a
b
Phytoplankton (x10^5 ml^{-1})
Eukaryotes (x10^4 ml^{-1})
0
2
4
6
0
4
8
12
16
-2
1
4
7
10
13
16
19
22
25
28
31
34
37
Time (days)

Figure 1.

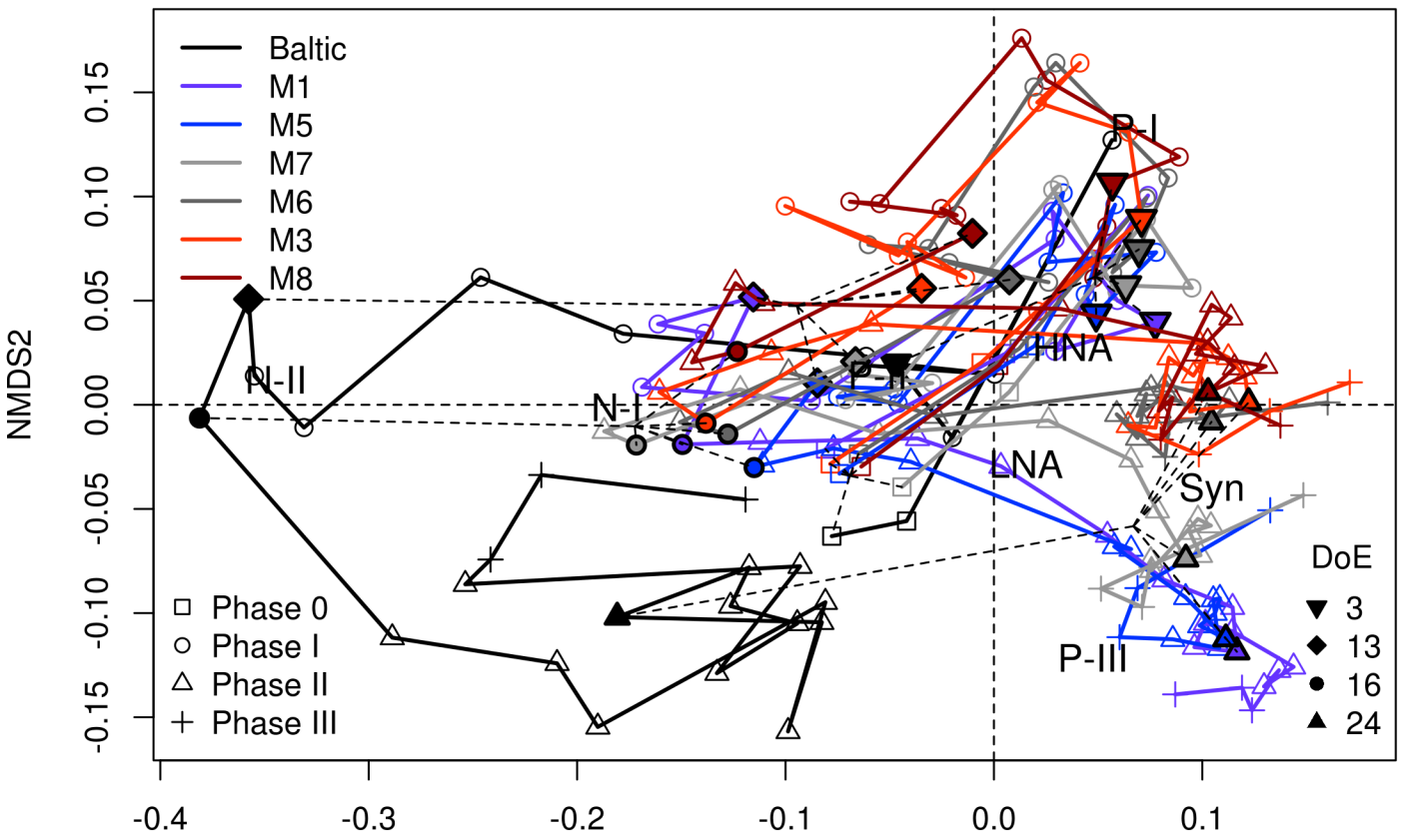
Baltic
M1
M5
M7
M6
M3
M8
P-I
HNA
N-II
N-I
NA
Syn
P-III
DoE
3
13
16
24
Phase 0
Phase I
Phase II
Phase III
NMDS2
0.15
0.10
0.05
0.00
-0.05
-0.10
-0.15
-0.4
-0.3
-0.2
-0.1
0.0
0.1

Figure 2.

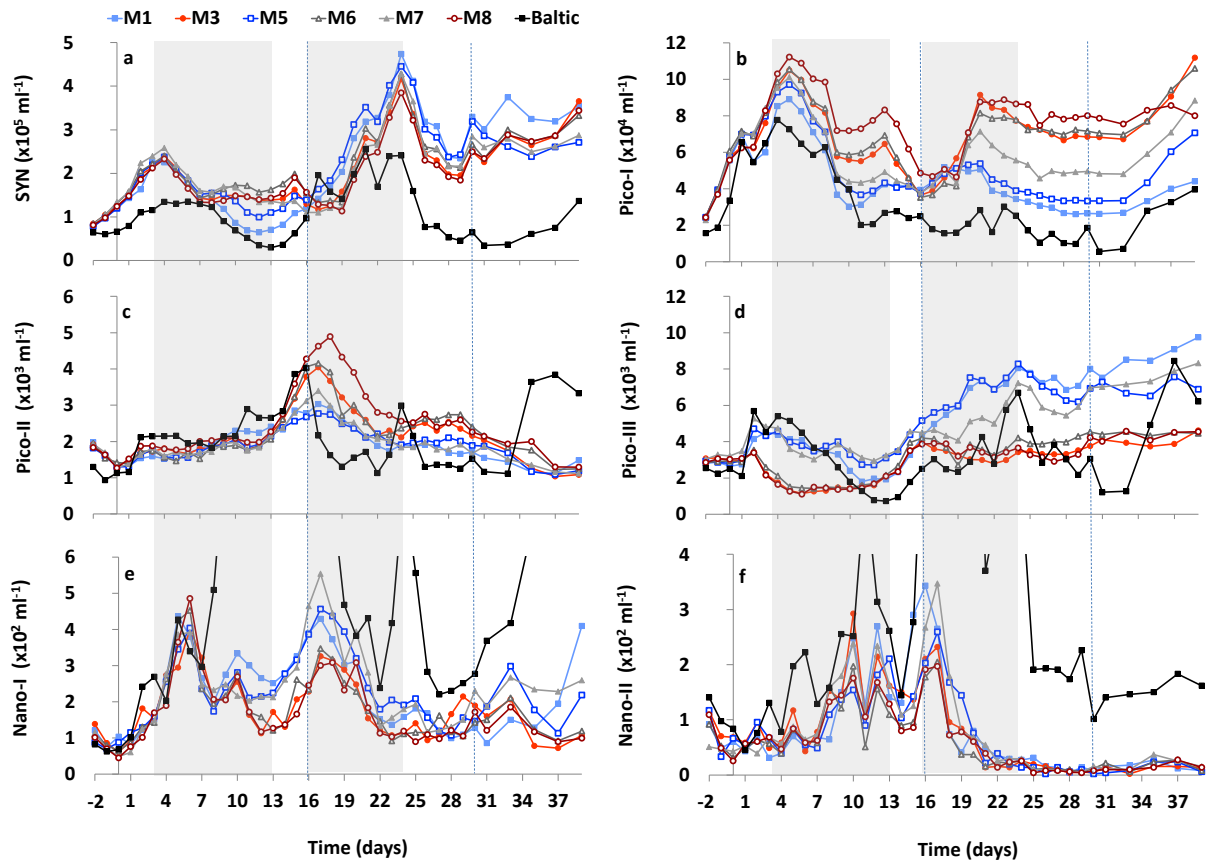
M1
M3
M5
M6
M7
M8
Baltic
a
b
c
d
e
f
SYN (x10⁵ ml⁻¹)
Pico-I (x10⁴ ml⁻¹)
Pico-II (x10³ ml⁻¹)
Pico-III (x10³ ml⁻¹)
Nano-I (x10² ml⁻¹)
Nano-II (x10² ml⁻¹)
-2 1 4 7 10 13 16 19 22 25 28 31 34 37
Time (days)

Figure 3.

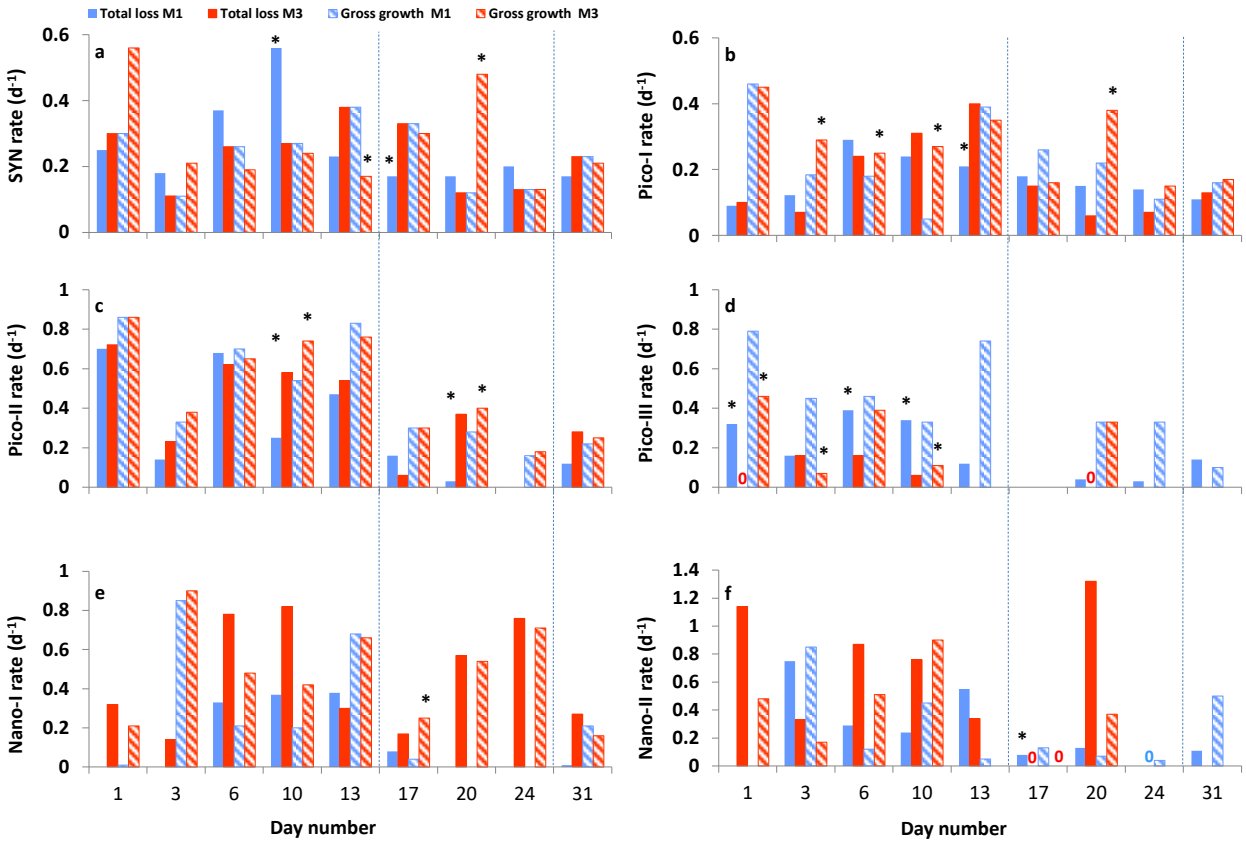
Total loss M1
Total loss M3
Gross growth M1
Gross growth M3
a
b
c
d
e
f
SYN rate (d-1)
Pico-I rate (d-1)
Pico-II rate (d-1)
Pico-III rate (d-1)
Nano-I rate (d-1)
Nano-II rate (d-1)
Day number
Day number

Figure 4.

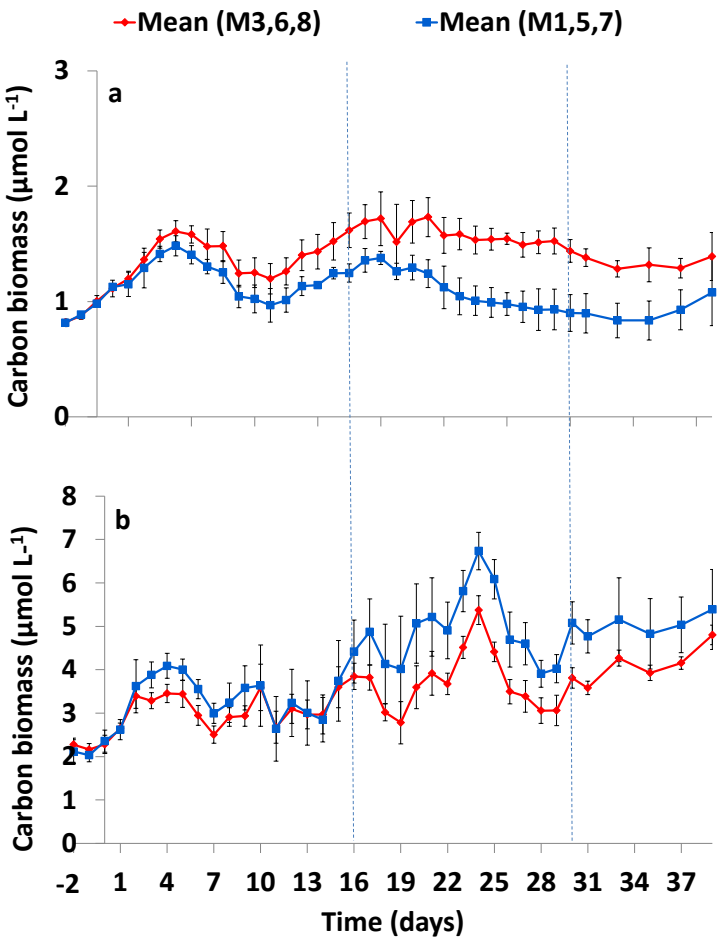
Mean (M3,6,8)
Mean (M1,5,7)
a
b
Carbon biomass (µmol L-1)
Carbon biomass (µmol L-1)
Time (days)

Figure 5.

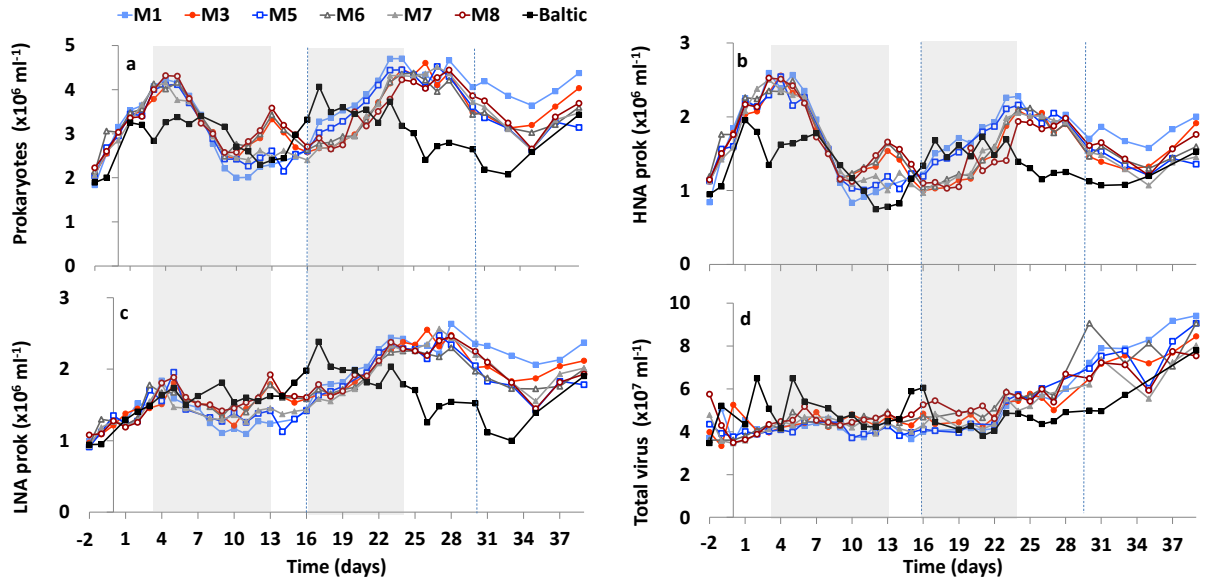
M1
M3
M5
M6
M7
M8
Baltic
a
b
c
d
Prokaryotes (x10⁶ ml⁻¹)
HNA prok (x10⁶ ml⁻¹)
LNA prok (x10⁶ ml⁻¹)
Total virus (x10⁷ ml⁻¹)
Time (days)
Time (days)

Figure 6.

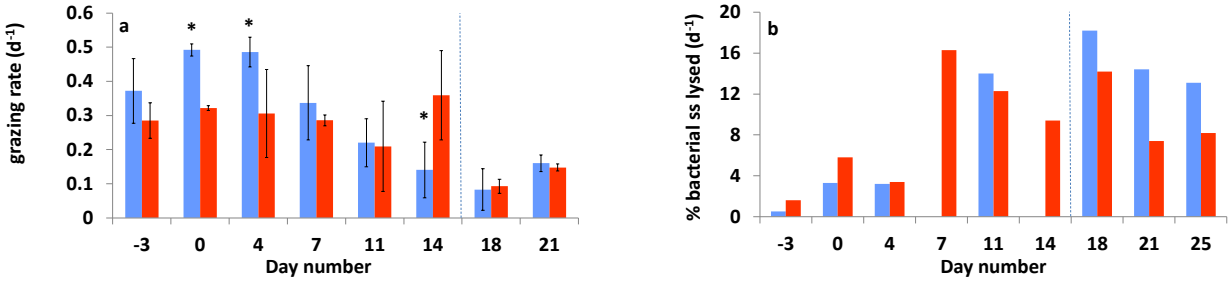
a
grazing rate (d-1)
0.6
0.5
0.4
0.3
0.2
0.1
0
*
*
*
-3
0
4
7
11
14
18
21
Day number
b
% bacterial ss lysed (d-1)
20
16
12
8
4
0
-3
0
4
7
11
14
18
21
25
Day number

Figure 7.

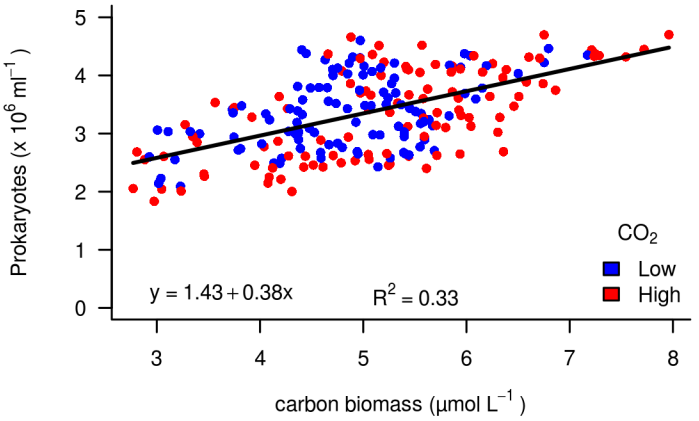
Prokaryotes (x 10^6 ml^-1)
carbon biomass (µmol L^-1)
y = 1.43 + 0.38x
R^2 = 0.33
CO2
Low
High

Figure 8.